AUT Journal of Mechanical Engineering

AUT J. Mech. Eng., 2(2) (2018) 177-190
DOI: 10.22060/ajme.2018.13624.5687

Surface stress effect on nonlinear instability of imperfect piezoelectric nanoshells under combination of hydrostatic pressure and lateral electric field

S. Sahmani[1*], M.M. Aghdam[1], A.H. Akbarzadeh[2,3]

[1] Department of Mechanical Engineering, Amirkabir University of Technology, Tehran, Iran
[2] Department of Bioresource Engineering, McGill University, Ste-Anne-de-Bellevue, Island of Montreal, Canada
[3] Department of Mechanical Engineering, McGill University, Montreal, Canada

ABSTRACT: In this paper, the nonlinear instability of piezoelectric cylindrical nanoshells under the combined radial compression and electrical load including the effects of surface free energy is studied. To consider the surface effects, the Gurtin-Murdoch elasticity theory is utilized along with the classical shell theory to develop an efficient size-dependent shell model. To satisfy the balance conditions on the surfaces of nanoshells, a linear variation of normal stress is assumed through the thickness of the bulk. Electrical field is also exerted along the transverse direction. Based on the virtual work principle, the size-dependent nonlinear governing differential equations are derived in which transverse displacement and Airy stress function are considered as independent variables. After that, a boundary layer theory is used incorporating the surface free energy effects in conjunction with the nonlinear prebuckling deformation, the large deflections in the postbuckling regime, and the initial geometrical imperfection. Finally, a two-stepped singular perturbation technique is employed to obtain the size-dependent critical buckling pressure and the associated postbuckling equilibrium path for alternative electrical loadings. It is revealed that the electrical load increases or decreases the critical buckling pressure and critical end-shortening of nanoshell which depends on the sign of applied voltage. Moreover, it is found that by taking surface free energy effects into account, the influence of electrical load on the postbuckling behavior of nanoshell increases.

Review History:
Received: 6 November 2017
Revised: 17 January 2018
Accepted: 31 January 2018
Available Online: 20 February 2018

Keywords:
Nanomechanics
Piezoelectric material
Nonlinear buckling
Size effect
Surface elasticity theory

1- Introduction

Due to the distinguished thermophysical properties of nano-structured elements, they have found wide range of applications in medicine, aerospace, automotive, and agriculture which make them as the substantial building blocks for various nanosystems and nanodevives. Nanostructures have shown size-dependent properties. The classical continuum mechanics is a scale-independent theory. As a result, some modified continuum theories have been developed to characterize the size effect observed in nanoscale structures. Several studies have been conducted in which the proposed modified continuum theories have been utilized as a bridge between the physics features at macroscale and nanoscale. Strain gradient elasticity theory, couple stress elasticity theory, and nonlocal elasticity theory are examples of these non-classical theories which have been employed in several investigations. For example, Hu et al. [1] investigated the transverse and torsional wave in carbon nanotubes based on nonlocal shell model. Shen and Zhang [2] explored the torsional nonlinear instability of carbon nanotubes via nonlocal shear deformable shell model. Wang et al. [3] developed a size-dependent Timoshenko beam model on the basis of the strain gradient elasticity theory. Ansari et al. [4] proposed a calibrated nonlocal plate model for free vibration analysis of graphene sheets. Khademolhosseini et al. [5] used nonlocal elasticity theory for the size-dependent torsional buckling analysis of carbon nanotubes. Shen and Zhang [6] proposed a nonlocal beam model for nonlinear mechanical behavior of carbon nanotubes embedded in elastomeric substrates. Ahangar et al. [7] analyzed the stability of a microbeam conveying fluid based upon the modified couple stress elasticity theory. Ghavanloo and Fazelzadeh [8] constructed a nonlocal shell model for radial vibrations of spherical shells at nanoscale. Shen [9] studied the torsional postbuckling response of microtubules via nonlocal elastic shell model. Ghanbarpour Arani et al. [10] predicted the nonlocal piezoelasticity based wave propagation of bonded double-piezoelectric nanobeam-system. Sahmani et al. [11] employed the modified strain gradient elasticity theory for the nonlinear vibrational response of functionally graded microbeams. Mustapha and Ruan [12] anticipated size dependency in axial dynamics of magnetically-sensitive strain gradient microbars with end attachments. Sahmani and Bahrami [13] utilized the strain gradient continuum theory for dynamic stability analysis of microbeams actuated by piezoelectric voltage. Sari and Al-Kouz [14] reported the nonlocal natural frequencies of non-uniform orthotropic Kirchhoff plates resting on an elastic foundation. Aydogdu and Arda [15] investigated the torsional vibration characteristics of double-walled carbon nanotubes based on the nonlocal theory of elasticity. Sahmani and Aghdam [16-18] employed the nonlocal continuum theory to study the nonlinear instability of hybrid functionally graded nanoshells under different loading conditions. Mohammadimehr et al. [19] examined the size-dependent free vibrations of double-bonded isotropic piezoelectric Timoshenko microbeam under initial stress. Sahmani and Aghdam [20, 21] analyzed the linear and nonlinear vibrations of pre- and post-buckled lipid micro/nano-tubules based on the nonlocal strain gradient

Corresponding author, E-mail: sahmani@aut.ac.ir

elasticity theory. Lu et al. [22] employed the nonlocal strain gradient theory of elasticity to capture size effects on the free vibration behavior of nanobeams. Sahmani and Aghdam [23] predicted the size-dependent nonlinear bending of nanobeams made of nanoporous biomaterials. El-Borgi et al. [24] analyzed the torsional vibration of size-dependent viscoelastic rods. Sahmani and Aghdam [25] and Sahmani et al. [26] utilized the nonlocal strain gradient continuum mechanics for the size-dependent nonlinear instability of smart and porous micro/nano-structures.

Because of different environmental conditions, the equilibrium requirements relevant to the atoms on the free surfaces of a structure are different from those of the bulk. This difference leads to create an extra energy namely as surface free energy. The effect of surface free energy causes different material properties for the boundary layers of the structure. As a result, because by decreasing the scale of a structure, the ratio of surface area to volume increases, surface free energy effect plays an important role in the mechanical characteristics of nanostructures which yields size-dependent behavior. For this reason, Gurtin and Murdoch [27, 28] proposed a generic theoretical framework based on the concepts of continuum mechanics that accounts surface free energy. Based upon their surface elasticity theory, the surface layer of a solid can be modeled as a mathematical layer of zero thickness having different material properties from the underlying bulk which is perfectly attached to the membrane. In recent years, several investigations been carried out in which Gurtin-Murdoch elasticity theory has been used in connection with the mechanical behavior of nanostructures.

Lim and He [29] developed a size-dependent model to analyze the geometrically nonlinear response of thin elastic films with nanoscale thickness on the basis of continuum approach using surface elasticity theory. Li et al. [30] studied the influence of surface free energy on the stress concentration around a spherical cavity in a linearly isotropic elastic medium based upon surface elasticity theory. Wang and Feng [31] extended the surface elastic model to investigate the surface stress effects on contact problems based on a closed-form solution. He and Lilley [32] reported the effects of surface stress on the static bending and bending resonance of nanowires with various boundary conditions. By using Gurtin-Murdoch elasticity theory, Mogilevskaya et al. [33] solved a two-dimensional problem of multiple interacting circular nano-inhomogeneities and nano-pores. Zhao and Rajapakse [34] examined the plane and axisymmetric problems corresponding to a surface-loaded elastic layer including effects of surface free energy. Fu et al. [35] investigated the influences of surface free energy on the free vibration and buckling behavior of nanobeams in the both linear and nonlinear regimes using Galerkin's technique. Through incorporation Gurtin-Murdoch elasticity theory into the different types of beam theory, Ansari and Sahmani [36] predicted the bending and buckling behavior of nanoscale beams in the presence of surface stress effects. Also, Ansari and Sahmani [37] studied the free vibration response of rectangular nanoplates based on surface elasticity theory and within the framework of different plate theories. Wang [38] investigated the postbuckling characteristics of nanobeams containing internal flowing fluid incorporating the effects of surface stress. Liu et al. [39] analyzed the propagation of shear horizontal waves in an ultra-thin plate-like film with nanoscale thickness including surface stress effects within the framework of a theoretical solution. Khater et al. [40] investigated the impact of surface free energy and thermal loading on the static stability of curved nanowires. Gao et al. [41] considered the surface stress effects in the analysis of nanowire buckling on elastomeric substrate. Sahmani et al. [42] developed a non-classical beam model to study the nonlinear forced vibrations of nanobeams on the basis of surface elasticity theory. Sahmani et al. [43] presented the surface stress effects on the free vibration response of postbuckled circular higher-order shear deformable nanoplates based on Gurtin-Murdoch elasticity theory. Zhang et al. [44] implemented the high-order surface stress model into the Bernoulli-Euler beam theory to analyze the transverse vibration of an axially compressed nanowire embedded in elastic medium. Sahmani et al. [45] achieved the natural frequencies of postbuckled third-order shear deformable nanobeams made of functionally graded materials including the effects of surface free energy. Liang et al. [46] proposed a theoretical model to study the effects of surface stress on the postbuckling behavior of piezoelectric nanowires. Abdel Rahman et al. [47] developed a nonlinear finite element model to anticipate the quasistatic response of nanoindentation problems of an elastically-layered viscoelastic material considering the surface elasticity effects. Sahmani and Aghdam [49] and Sahmani et al. [48, 50-52] studied the surface stress size dependency in the buckling and postbuckling characteristics of nanoshells under different loading conditions.

The objective of the present study is to examine the nonlinear instability of piezoelectric cylindrical nanoshells subjected to combined radial compression and electrical load in the presence of surface free energy effects. To this end, an efficient size-dependent shell model is developed through implementing of Gurtin-Murdoch elasticity theory into the classical shell theory. On the basis of the variational approach using the principle of virtual work, the non-classical governing differential equations are derived. Subsequently, a boundary layer theory is utilized incorporating the surface free energy effects in addition to the nonlinear prebuckling deformation, the large deflections in the postbuckling regime, and the initial geometrical imperfection. Then a solution methodology based on a two-stepped singular perturbation technique is put to use to obtain the size-dependent critical buckling pressure and associated postbuckling equilibrium path of piezoelectric cylindrical nanoshells.

2- Problem Definition and Governing Equations

As it can be seen in Fig. 1, a cylindrical nanoshell made of PZT-5H piezoelectric material with the length L, thickness h, and mid-surface radius R subjected to hydrostatic pressure combined with electrical field is considered. A bulk part and two additional thin surface layers (inner and outer layers) are different parts of the nanoshell. The material properties associated with the bulk part include the Young's modulus E and Poisson's ratio ν. The two additional surface layers are assumed to have surface elasticity modulus of E_s, Poisson's ratio ν_s and the surface residual tension τ_s. On the basis of a curvilinear coordinate system depicted in Fig.1, whose origin is located on the middle surface of the nanoshell, the coordinates of a typical point in the axial, circumferential and radial directions are represented by x, y and z, respectively. Now, based upon the classical shell theory, the displacement

field for an imperfect nanoshell can be given as

$$u_x(x,y,z)=u(x,y)-z\frac{\partial w(x,y)}{\partial x} \tag{1-a}$$

$$u_y(x,y,z)=v(x,y)-z\frac{\partial w(x,y)}{\partial y} \tag{1-b}$$

$$u_z(x,y,z)=w(x,y)+w^*(x,y) \tag{1-c}$$

where u, v and w are the displacements of middle plane along x, y and z axis, respectively; w^* stands for the initial geometric imperfection.

Based upon the von Karman-Donnell-type kinematics of nonlinearity [53], in which it is assumed that the thickness of the shell h, is remarkably small compared to its radius of curvature R, the relations of strain-displacement for an imperfect piezoelectric cylindrical nanoshell subjected to an external electrical field through thickness direction (E_z) can be written as

$$\begin{Bmatrix}\varepsilon_{xx}\\ \varepsilon_{yy}\\ \gamma_{xy}\end{Bmatrix}=\begin{Bmatrix}\varepsilon_{xx}^{M}\\ \varepsilon_{yy}^{M}\\ \gamma_{xy}^{M}\end{Bmatrix}+\begin{Bmatrix}\varepsilon_{xx}^{E}\\ \varepsilon_{yy}^{E}\\ \gamma_{xy}^{E}\end{Bmatrix}=\begin{Bmatrix}\varepsilon_{xx}^{0}\\ \varepsilon_{yy}^{0}\\ \gamma_{xy}^{0}\end{Bmatrix}+z\begin{Bmatrix}\kappa_{xx}\\ \kappa_{yy}\\ \kappa_{xy}\end{Bmatrix}+\begin{Bmatrix}\frac{d_{31}\mathcal{V}}{h}\\ \frac{d_{31}\mathcal{V}}{h}\\ 0\end{Bmatrix}$$

$$=\begin{Bmatrix}\frac{\partial u}{\partial x}+\frac{1}{2}\left(\frac{\partial w}{\partial x}\right)^2+\frac{\partial w}{\partial x}\frac{\partial w^*}{\partial x}\\ \frac{\partial v}{\partial y}-\frac{w+w^*}{R}+\frac{1}{2}\left(\frac{\partial w}{\partial y}\right)^2+\frac{\partial w}{\partial y}\frac{\partial w^*}{\partial y}\\ \frac{\partial u}{\partial y}+\frac{\partial v}{\partial x}+\frac{\partial w}{\partial x}\frac{\partial w}{\partial y}+\frac{\partial w}{\partial x}\frac{\partial w^*}{\partial y}+\frac{\partial w}{\partial y}\frac{\partial w^*}{\partial x}\end{Bmatrix}-z\begin{Bmatrix}\frac{\partial^2 w}{\partial x^2}\\ \frac{\partial^2 w}{\partial y^2}\\ 2\frac{\partial^2 w}{\partial x\,\partial y}\end{Bmatrix}+\begin{Bmatrix}\frac{d_{31}\mathcal{V}}{h}\\ \frac{d_{31}\mathcal{V}}{h}\\ 0\end{Bmatrix} \tag{2}$$

where ε_{xx}^{M}, ε_{yy}^{M}, γ_{xy}^{M} and ε_{xx}^{E}, ε_{yy}^{E}, γ_{xy}^{E} are, respectively, the mechanical and electrical strain components. Also, ε_{xx}^{0}, ε_{yy}^{0}, γ_{xy}^{0} represent the middle plane strain components, and κ_{xx}, κ_{yy}, κ_{xy} denote the curvature components of the nanoshell. Moreover, d_{31} and $\mathcal{V}=E_z h$ are the piezoelectric strain constant and applied voltage across the shell thickness, respectively.

After that, the constitutive relations related to an elastic material can be expressed as

$$\begin{Bmatrix}\sigma_{xx}\\ \sigma_{yy}\\ \sigma_{xy}\end{Bmatrix}=\begin{bmatrix}\lambda+2\mu & \lambda & 0\\ \lambda & \lambda+2\mu & 0\\ 0 & 0 & \mu\end{bmatrix}\begin{Bmatrix}\varepsilon_{xx}^{M}\\ \varepsilon_{yy}^{M}\\ \gamma_{xy}^{M}\end{Bmatrix}-\begin{bmatrix}\lambda+2\mu & \lambda & 0\\ \lambda & \lambda+2\mu & 0\\ 0 & 0 & \mu\end{bmatrix}\begin{bmatrix}1 & 0\\ 0 & 1\\ 0 & 0\end{bmatrix}\begin{Bmatrix}\frac{d_{31}\mathcal{V}}{h}\\ \frac{d_{31}\mathcal{V}}{h}\end{Bmatrix} \tag{3}$$

in which $\lambda=Ev/(1-v^2)$ and $\mu=E/(2(1+v))$ are Lame's constants. An efficient way to consider the effects of surface free energy in the conventional continuum mechanics is using Gurtin-Murdoch elasticity theory. Due to the atomic features observed in nanostructures, the elastic surface and bulk material are affected by each other. Therefore, structures at nanoscale are mostly subjected to in-plane loads in different directions. These in-plane loads acted on the surfaces a nanoshell lead to a kind of surface stress, the relation of which with respect to the strain components can be determined based on the constitutive equation developed by the Gurtin-Murdoch elasticity theory as below [27, 28]

$$\begin{aligned}&\sigma_{ij}^{s}=\tau_s\delta_{ij}+(\tau_s+\lambda_s)\varepsilon_{kk}\delta_{ij}\\ &+2(\mu_s-\tau_s)\varepsilon_{ij}+\tau_s u_{i,j}^{s}\qquad;(i,j=x,y)\\ &\sigma_{iz}^{s}=\tau_s u_{z,i}^{s}\end{aligned} \tag{4}$$

where λ_s and μ_s stand for the surface Lame's constants and τ_s is the residual surface stress under unstrained conditions. As a result, the surface stress components with respect to the displacement field can be derived as

$$\begin{aligned}&\sigma_{xx}^{s}=(\lambda_s+2\mu_s)\left(\varepsilon_{xx}^{M}-\frac{d_{31}\mathcal{V}}{h}\right)\\ &+(\tau_s+\lambda_s)\left(\varepsilon_{yy}^{M}-\frac{d_{31}\mathcal{V}}{h}\right)+\tau_s-\frac{\tau_s}{2}\left(\frac{\partial(w+w^*)}{\partial x}\right)^2\\ &\sigma_{yy}^{s}=(\lambda_s+2\mu_s)\left(\varepsilon_{yy}^{M}-\frac{d_{31}\mathcal{V}}{h}\right)\\ &+(\tau_s+\lambda_s)\left(\varepsilon_{xx}^{M}-\frac{d_{31}\mathcal{V}}{h}\right)+\frac{\tau_s}{R}(w+w^*)\\ &+\tau_s-\frac{\tau_s}{2}\left(\frac{\partial(w+w^*)}{\partial y}\right)^2\\ &\sigma_{xy}^{s}=\mu_s\gamma_{xy}^{M}-\tau_s\left(\frac{\partial v}{\partial x}+\frac{\partial(w+w^*)}{\partial x}\frac{\partial(w+w^*)}{\partial y}-z\frac{\partial^2 w}{\partial x\,\partial y}\right)\\ &\sigma_{yx}^{s}=\mu_s\gamma_{xy}^{M}-\tau_s\left(\frac{\partial u}{\partial y}+\frac{\partial(w+w^*)}{\partial x}\frac{\partial(w+w^*)}{\partial y}-z\frac{\partial^2 w}{\partial x\,\partial y}\right)\\ &\sigma_{xz}^{s}=\tau_s\frac{\partial w}{\partial x}\quad,\quad\sigma_{yz}^{s}=\tau_s\frac{\partial w}{\partial y}\end{aligned} \tag{5}$$

In comparison with other stress components, the normal bulk stress component σ_{zz} is small based on the classical continuum theory. As a result, it is assumed that $\sigma_{zz}=0$. Nevertheless, the surface conditions relevant to the Gurtin-Murdoch model

cannot be satisfied by this simplification. In order to solve this problem, a linear variation of the stress component σ_{zz} through the shell thickness is supposed in such a way that satisfies the balance conditions on the surfaces of nanoshell. In accordance with this assumption, one will have

$$\sigma_{zz}=\frac{\left(\frac{\partial\sigma_{xz}^{S+}}{\partial x}+\frac{\partial\sigma_{yz}^{S+}}{\partial y}\right)-\left(\frac{\partial\sigma_{xz}^{S-}}{\partial x}+\frac{\partial\sigma_{yz}^{S-}}{\partial y}\right)}{2}+\frac{\left(\frac{\partial\sigma_{xz}^{S+}}{\partial x}+\frac{\partial\sigma_{yz}^{S+}}{\partial y}\right)+\left(\frac{\partial\sigma_{xz}^{S-}}{\partial x}+\frac{\partial\sigma_{yz}^{S-}}{\partial y}\right)}{h}z \tag{6}$$

in which the superscripts S^+ and S^- refer to the outer and inner surfaces of nanoshell, respectively. By inserting Eq. (5) into Eq. (6), σ_{zz} can be achieved as

$$\sigma_{zz}=\frac{2\tau_s z}{h}\left(\frac{\partial^2 w}{\partial x^2}+\frac{\partial^2 w}{\partial y^2}\right) \tag{7}$$

Now, by substituting the σ_{zz} in the constitutive equation (Eq. (3)) relevant to the normal stresses (σ_{xx} , σ_{yy}) of the bulk, it yields

$$\sigma_{xx}=(\lambda+2\mu)\left(\varepsilon_{xx}^{M}-\frac{d_{31}\mathcal{V}}{h}\right)+\lambda\left(\varepsilon_{yy}^{M}-\frac{d_{31}\mathcal{V}}{h}\right)+\frac{\nu\sigma_{zz}}{(1-\nu)} \tag{8-a}$$

$$\sigma_{yy}=(\lambda+2\mu)\left(\varepsilon_{yy}^{M}-\frac{d_{31}\mathcal{V}}{h}\right)+\lambda\left(\varepsilon_{xx}^{M}-\frac{d_{31}\mathcal{V}}{h}\right)+\frac{\nu\sigma_{zz}}{(1-\nu)} \tag{8-b}$$

Based upon the surface elasticity theory, the total strain energy of a piezoelectric cylindrical nanoshell incorporating the surface free energy effects can be given as

$$\Pi_s=\frac{1}{2}\int_S\int_{-\frac{h}{2}}^{\frac{h}{2}}\sigma_{ij}\varepsilon_{ij}dzdS+\frac{1}{2}\left(\int_{S^+}\sigma_{ij}^{s}\varepsilon_{ij}dS^{+}+\int_{S^-}\sigma_{ij}^{s}\varepsilon_{ij}dS^{-}\right)$$
$$=\frac{1}{2}\int_S\left\{\bar{N}_{xx}\left(\varepsilon_{xx}^{0}+\frac{d_{31}\mathcal{V}}{h}\right)+\bar{N}_{yy}\left(\varepsilon_{yy}^{0}+\frac{d_{31}\mathcal{V}}{h}\right)+\bar{N}_{xy}\gamma_{xy}^{0}+\bar{M}_{xx}\kappa_{xx}+\bar{M}_{yy}\kappa_{yy}+\bar{M}_{xy}\kappa_{xy}+Q_x^{s}\frac{\partial w}{\partial x}+Q_y^{s}\frac{\partial w}{\partial y}\right\}dS \tag{9}$$

where S is the area occupied by the middle plane of the nanoshell. The in-plane forces, bending moments and shear forces presented in Eq. (9) can be defined as

$$\bar{N}_{xx}=N_{xx}+\sigma_{xx}^{s+}+\sigma_{xx}^{s-}=A_{11}^{*}\varepsilon_{xx}^{0}+A_{12}^{*}\varepsilon_{yy}^{0}+2\tau_s-\tau_s\left(\frac{\partial\left(w+w^{*}\right)}{\partial x}\right)^2-N^{E} \tag{10}$$

$$\bar{N}_{yy}=N_{yy}+\sigma_{yy}^{s+}+\sigma_{yy}^{s-}=A_{11}^{*}\varepsilon_{yy}^{0}+A_{12}^{*}\varepsilon_{xx}^{0}+\frac{2\tau_s}{R}\left(w+w^{*}\right)+2\tau_s-\tau_s\left(\frac{\partial\left(w+w^{*}\right)}{\partial y}\right)^2-N^{E}$$

$$\bar{N}_{xy}=N_{xy}+\frac{1}{2}\left(\sigma_{xy}^{s+}+\sigma_{yx}^{s+}+\sigma_{xy}^{s-}+\sigma_{yx}^{s-}\right)=A_{55}^{*}\gamma_{xy}^{0}-\tau_s\frac{\partial\left(w+w^{*}\right)}{\partial x}\frac{\partial\left(w+w^{*}\right)}{\partial y}$$

$$\bar{M}_{xx}=M_{xx}+\frac{h}{2}\left(\sigma_{xx}^{s+}-\sigma_{xx}^{s-}\right)=D_{11}^{*}\kappa_{xx}+D_{12}^{*}\kappa_{yy}+E_{11}^{*}\left(\frac{\partial^2 w}{\partial x^2}+\frac{\partial^2 w}{\partial y^2}\right)$$

$$\bar{M}_{yy}=M_{yy}+\frac{h}{2}\left(\sigma_{yy}^{s+}-\sigma_{yy}^{s-}\right)=D_{11}^{*}\kappa_{yy}+D_{12}^{*}\kappa_{xx}+E_{11}^{*}\left(\frac{\partial^2 w}{\partial x^2}+\frac{\partial^2 w}{\partial y^2}\right)$$

$$\bar{M}_{xy}=M_{xy}+\frac{h}{4}\left(\sigma_{xy}^{s+}+\sigma_{yx}^{s+}-\sigma_{xy}^{s-}-\sigma_{yx}^{s-}\right)=D_{55}^{*}\kappa_{xy}$$

$$Q_x^{s}=\sigma_{xz}^{s-}+\sigma_{xz}^{s+}=2\tau_s\frac{\partial w}{\partial x}$$

$$Q_y^{s}=\sigma_{yz}^{s-}+\sigma_{yz}^{s+}=2\tau_s\frac{\partial w}{\partial y}$$

in which

$$\begin{Bmatrix}N_{xx}\\N_{yy}\\N_{xy}\end{Bmatrix}=\int_{-\frac{h}{2}}^{\frac{h}{2}}\begin{Bmatrix}\sigma_{xx}\\\sigma_{yy}\\\sigma_{xy}\end{Bmatrix}dz$$
$$\begin{Bmatrix}M_{xx}\\M_{yy}\\M_{xy}\end{Bmatrix}=\int_{-\frac{h}{2}}^{\frac{h}{2}}\begin{Bmatrix}\sigma_{xx}\\\sigma_{yy}\\\sigma_{xy}\end{Bmatrix}zdz \tag{11}$$
$$N^{E}=\frac{\left(A_{11}^{*}+A_{12}^{*}\right)d_{13}\mathcal{V}}{h}$$

and

$$A_{11}^{*}=(\lambda+2\mu)h+2\left(\lambda_s+2\mu_s\right)$$
$$A_{12}^{*}=\lambda h+2\tau_s+2\lambda_s$$
$$A_{55}^{*}=\mu h+2\mu_s-\tau_s$$
$$D_{11}^{*}=\frac{(\lambda+2\mu)h^3}{12}+\frac{\left(\lambda_s+2\mu_s\right)h^2}{2} \tag{12}$$
$$D_{12}^{*}=\frac{\lambda h^3}{12}+\frac{\left(\tau_s+\lambda_s\right)h^2}{2}$$

$$E_{11}^{*}=\frac{\nu h^{2}\tau_{s}}{6(1-\nu)}$$

$$D_{55}^{*}=\frac{\mu h^{3}}{12}+\frac{(2\mu_{s}-\tau_{s})h^{2}}{4}$$

Moreover, the work Π_P done by the external radial load q can be obtained as

$$\Pi_{P}=\int_{S}qwdS \tag{13}$$

Now, by using the principle of virtual work as below

$$\delta\int_{t_1}^{t_2}(\Pi_{s}-\Pi_{P})\,\mathrm{d}t=0 \tag{14}$$

and taking the variation of u, v, and w and integrating by parts, the non-classical governing differential equations can be derived in the following form

$$\frac{\partial\bar{N}_{xx}}{\partial x}+\frac{\partial\bar{N}_{xy}}{\partial y}=0 \tag{15-a}$$

$$\frac{\partial\bar{N}_{xy}}{\partial x}+\frac{\partial\bar{N}_{yy}}{\partial y}=0 \tag{15-b}$$

$$\begin{aligned}&\frac{\partial^{2}\bar{M}_{xx}}{\partial x^{2}}+2\frac{\partial^{2}\bar{M}_{xy}}{\partial x\,\partial y}+\frac{\partial^{2}\bar{M}_{yy}}{\partial y^{2}}+\frac{\partial Q_{x}^{s}}{\partial x}\\&+\frac{\partial Q_{y}^{s}}{\partial y}+\frac{\bar{N}_{yy}}{R}+\bar{N}_{xx}\frac{\partial^{2}w}{\partial x^{2}}+2\bar{N}_{xy}\frac{\partial^{2}w}{\partial x\,\partial y}\\&+\bar{N}_{yy}\frac{\partial^{2}w}{\partial y^{2}}+q=0\end{aligned} \tag{15-c}$$

The Airy stress function $f(x,y)$ can be introduced as

$$\bar{N}_{xx}=\frac{\partial^{2}f}{\partial y^{2}}\quad,\quad\bar{N}_{yy}=\frac{\partial^{2}f}{\partial x^{2}}\quad,\quad\bar{N}_{xy}=-\frac{\partial^{2}f}{\partial x\,\partial y} \tag{16}$$

As a result, the strain components of middle plane can be derived as

$$\begin{aligned}\varepsilon_{xx}^{0}&=-\varphi_{2}\frac{\partial^{2}f}{\partial x^{2}}+\varphi_{1}\frac{\partial^{2}f}{\partial y^{2}}+2\tau_{s}\varphi_{2}\frac{w+w^{*}}{R}\\&-\frac{2\tau_{s}}{A_{11}^{*}+A_{12}^{*}}+\tau_{s}\varphi_{1}\left(\frac{\partial(w+w^{*})}{\partial x}\right)^{2}\\&-\tau_{s}\varphi_{2}\left(\frac{\partial(w+w^{*})}{\partial y}\right)^{2}+(\varphi_{1}-\varphi_{2})N^{E}\end{aligned} \tag{17-a}$$

$$\begin{aligned}\varepsilon_{yy}^{0}&=-\varphi_{2}\frac{\partial^{2}f}{\partial y^{2}}+\varphi_{1}\frac{\partial^{2}f}{\partial x^{2}}-2\tau_{s}\varphi_{1}\frac{w+w^{*}}{R}\\&-\frac{2\tau_{s}}{A_{11}^{*}+A_{12}^{*}}+\tau_{s}\varphi_{1}\left(\frac{\partial(w+w^{*})}{\partial y}\right)^{2}\\&-\tau_{s}\varphi_{2}\left(\frac{\partial(w+w^{*})}{\partial x}\right)^{2}+(\varphi_{1}-\varphi_{2})N^{E}\end{aligned} \tag{17-b}$$

$$\gamma_{xy}^{0}=-\varphi_{3}\frac{\partial^{2}f}{\partial x\,\partial y}+\tau_{s}\varphi_{3}\frac{\partial(w+w^{*})}{\partial x}\frac{\partial(w+w^{*})}{\partial y} \tag{17-c}$$

in which

$$\varphi_{1}=\frac{A_{11}^{*}}{(A_{11}^{*})^{2}-(A_{12}^{*})^{2}}\quad,\quad\varphi_{2}=\frac{A_{12}^{*}}{(A_{11}^{*})^{2}-(A_{12}^{*})^{2}}\quad,\quad\varphi_{3}=\frac{1}{A_{55}^{*}} \tag{18}$$

Moreover, the geometrical compatibility equation for an imperfect cylindrical shell can be expressed as

$$\begin{aligned}&\frac{\partial^{2}\varepsilon_{xx}^{0}}{\partial y^{2}}+\frac{\partial^{2}\varepsilon_{yy}^{0}}{\partial x^{2}}-\frac{\partial^{2}\gamma_{xy}^{0}}{\partial x\,\partial y}=\left(\frac{\partial^{2}w}{\partial x\,\partial y}\right)^{2}-\frac{\partial^{2}w}{\partial x^{2}}\frac{\partial^{2}w}{\partial y^{2}}\\&+2\frac{\partial^{2}w}{\partial x\,\partial y}\frac{\partial^{2}w^{*}}{\partial x\,\partial y}-\frac{\partial^{2}w}{\partial x^{2}}\frac{\partial^{2}w^{*}}{\partial y^{2}}-\frac{\partial^{2}w}{\partial y^{2}}\frac{\partial^{2}w^{*}}{\partial x^{2}}-\frac{1}{R}\frac{\partial^{2}w}{\partial x^{2}}\end{aligned} \tag{19}$$

With the aid of differential equations of Eqs. (15c) and (19) and in accordance with Eqs. (10) and (17), the size-dependent nonlinear governing differential equations can be derived as below

$$\begin{aligned}&\varphi_{4}\frac{\partial^{4}w}{\partial x^{4}}+2\varphi_{5}\frac{\partial^{4}(w+w^{*})}{\partial x^{2}\partial y^{2}}+\varphi_{4}\frac{\partial^{4}w}{\partial y^{4}}-2\tau_{s}\left(\frac{\partial^{2}w}{\partial x^{2}}+\frac{\partial^{2}w}{\partial y^{2}}\right)\\&-\frac{1}{R}\frac{\partial^{2}f}{\partial x^{2}}=\frac{\partial^{2}(w+w^{*})}{\partial x^{2}}\frac{\partial^{2}f}{\partial y^{2}}-2\frac{\partial^{2}(w+w^{*})}{\partial x\,\partial y}\frac{\partial^{2}f}{\partial x\,\partial y}\\&+\frac{\partial^{2}(w+w^{*})}{\partial y^{2}}\frac{\partial^{2}f}{\partial x^{2}}+q\end{aligned} \tag{20-a}$$

$$\begin{aligned}&\varphi_{1}\frac{\partial^{4}f}{\partial x^{4}}+(\varphi_{3}-2\varphi_{2})\frac{\partial^{4}f}{\partial x^{2}\partial y^{2}}+\varphi_{1}\frac{\partial^{4}f}{\partial y^{4}}\\&+\frac{2\tau_{s}}{R}\left(-\varphi_{1}\frac{\partial^{2}w}{\partial x^{2}}+\varphi_{2}\frac{\partial^{2}w}{\partial y^{2}}\right)+\frac{1}{R}\frac{\partial^{2}w}{\partial x^{2}}\\&=\left(\frac{\partial^{2}(w+w^{*})}{\partial x\,\partial y}\right)^{2}-\frac{\partial^{2}(w+w^{*})}{\partial x^{2}}\frac{\partial^{2}(w+w^{*})}{\partial y^{2}}\\&-2\tau_{s}\varphi_{1}\left(\frac{\partial^{3}(w+w^{*})}{\partial x\,\partial y^{2}}\frac{\partial(w+w^{*})}{\partial x}+2\left(\frac{\partial^{2}(w+w^{*})}{\partial x\,\partial y}\right)^{2}+\frac{\partial^{3}(w+w^{*})}{\partial x^{2}\partial y}\frac{\partial(w+w^{*})}{\partial y}\right)\\&+2\tau_{s}\varphi_{2}\left(\frac{\partial^{3}(w+w^{*})}{\partial x^{3}}\frac{\partial(w+w^{*})}{\partial x}+\frac{\partial^{3}(w+w^{*})}{\partial y^{3}}\frac{\partial(w+w^{*})}{\partial y}+\left(\frac{\partial^{2}(w+w^{*})}{\partial x^{2}}\right)^{2}+\left(\frac{\partial^{2}(w+w^{*})}{\partial y^{2}}\right)^{2}\right)\\&+\tau_{s}\varphi_{3}\left(\frac{\partial^{3}(w+w^{*})}{\partial x^{2}\partial y}\frac{\partial(w+w^{*})}{\partial y}+\frac{\partial^{2}(w+w^{*})}{\partial x^{2}}\frac{\partial^{2}(w+w^{*})}{\partial y^{2}}+\left(\frac{\partial^{2}(w+w^{*})}{\partial x\,\partial y}\right)^{2}+\frac{\partial(w+w^{*})}{\partial x}\frac{\partial^{3}(w+w^{*})}{\partial x\,\partial y^{2}}\right)\end{aligned} \tag{20-b}$$

where

$$\varphi_4 = D_{11}^* - E_{11}^* \quad , \quad \varphi_5 = D_{12}^* + D_{55}^* - E_{11}^* \tag{21}$$

The end supports of nanoshell are assumed to be clamped. Therefore, the necessary boundary conditions at x=0,L can be expressed as

For clamped edge supports: w=0, $\partial w/\partial x$=0

Additionally, it is clear that

$$\int_0^{2\pi R} \bar{N}_{xx} dy + \pi R^2 q = 0 \tag{22}$$

Additionally, the closed condition (periodicity condition) can be written as

$$\int_0^{2\pi R} \frac{\partial v}{\partial y} dy = 0 \tag{23-a}$$

which yields

$$\int_0^{2\pi R} \begin{Bmatrix} -\varphi_2 \frac{\partial^2 f}{\partial y^2} + \varphi_1 \frac{\partial^2 f}{\partial x^2} - 2\tau_s \varphi_1 \frac{w + w^*}{R} - \frac{2\tau_s}{A_{11}^* + A_{12}^*} + \tau_s \varphi_1 \left(\frac{\partial (w + w^*)}{\partial y} \right)^2 \\ -\tau_s \varphi_2 \left(\frac{\partial (w + w^*)}{\partial x} \right)^2 + \frac{w + w^*}{R} - \frac{1}{2} \left(\frac{\partial w}{\partial y} \right)^2 - \frac{\partial w}{\partial y} \frac{\partial w^*}{\partial y} + (\varphi_1 - \varphi_2) N^E \end{Bmatrix} dy = 0 \tag{23-b}$$

Furthermore, the average end shortening of nanoshell can be introduced as

$$\frac{\Delta_x}{L} = -\frac{1}{2\pi RL} \int_0^{2\pi RL} \frac{\partial u}{\partial x} dx dy = -\frac{1}{2\pi RL} \int_0^{2\pi RL} \begin{Bmatrix} -\varphi_2 \frac{\partial^2 f}{\partial x^2} + \varphi_1 \frac{\partial^2 f}{\partial y^2} + 2\tau_s \varphi_2 \frac{w + w^*}{R} - \frac{2\tau_s}{A_{11}^* + A_{12}^*} \\ +\varphi_1 \tau_s \left(\frac{\partial (w + w^*)}{\partial x} \right)^2 - \varphi_2 \tau_s \left(\frac{\partial (w + w^*)}{\partial y} \right)^2 - \frac{1}{2} \left(\frac{\partial w}{\partial x} \right)^2 - \frac{\partial w}{\partial x} \frac{\partial w^*}{\partial x} + (\varphi_1 - \varphi_2) N^E \end{Bmatrix} dx dy \tag{24}$$

3- Solution Procedure

3- 1- Boundary layer-type governing equations

At first, the following dimensionless parameters are defined to perform the solution methodology:

$$X = \frac{\pi x}{L} \quad , \quad Y = \frac{y}{R} \quad , \quad \beta = \frac{L}{\pi R}$$
$$\eta = \frac{L^2}{\pi^2 h^2} \quad , \quad \in = \frac{\pi^2 Rh}{L^2}$$
$$\left\{ a_{11}^*, a_{12}^*, a_{55}^*, d_{11}^*, d_{12}^*, d_{55}^*, e_{11}^* \right\} = \left\{ \frac{A_{11}^*}{A_{110}}, \frac{A_{12}^*}{A_{110}}, \frac{A_{55}^*}{A_{110}}, \frac{D_{11}^*}{A_{110} h^2}, \frac{D_{12}^*}{A_{110} h^2}, \frac{D_{55}^*}{A_{110} h^2}, \frac{E_{11}^*}{A_{110} h^2} \right\} \tag{25}$$
$$\{W, W^*\} = \frac{\partial}{h} \{w, w^*\} \quad , \quad F = \frac{\partial^2 f}{A_{110} h^2} \quad , \quad \bar{\tau} = \frac{\tau_s}{A_{110}}$$
$$\mathcal{P}_q = \frac{3^{3/4} q L R^{3/2}}{4\pi A_{110} h^{3/2}} \quad , \quad \delta_q = \frac{3^{3/4} \Delta_x \sqrt{R}}{4\pi h^{3/2}}$$

in which $A_{110}=(\lambda+2\mu)h$. Now, by introducing the derivative operators as below

$$\mathcal{L}_{11}(\ ) = \vartheta_4 \frac{\partial^4}{\partial X^4} + 2\vartheta_5 \beta^2 \frac{\partial^4}{\partial X^2 \partial Y^2} + \vartheta_4 \beta^4 \frac{\partial^4}{\partial Y^4}$$
$$\mathcal{L}_{12}(\ ) = -\eta \frac{\partial^2}{\partial X^2} - \eta \beta^2 \frac{\partial^2}{\partial Y^2}$$
$$\mathcal{L}_{21}(\ ) = \vartheta_1 \frac{\partial^4}{\partial X^4} + (\vartheta_3 - 2\vartheta_2) \beta^2 \frac{\partial^4}{\partial X^2 \partial Y^2} + \vartheta_1 \beta^4 \frac{\partial^4}{\partial Y^4}$$
$$\mathcal{L}_{22}(\ ) = -\vartheta_1 \frac{\partial^2}{\partial X^2} + \vartheta_2 \beta^2 \frac{\partial^2}{\partial Y^2}$$
$$\tilde{\mathcal{L}}_1(\ ) = \frac{\partial^2}{\partial X^2} \frac{\partial^2}{\partial Y^2} - 2 \frac{\partial^2}{\partial X \partial Y} \frac{\partial^2}{\partial X \partial Y} + \frac{\partial^2}{\partial Y^2} \frac{\partial^2}{\partial X^2}$$
$$\tilde{\mathcal{L}}_2(\ ) = \frac{\partial^3}{\partial X \partial Y^2} \frac{\partial}{\partial X} + \frac{\partial}{\partial X} \frac{\partial^3}{\partial X \partial Y^2} + 4 \frac{\partial^2}{\partial X \partial Y} \frac{\partial^2}{\partial X \partial Y} + \frac{\partial}{\partial Y} \frac{\partial^3}{\partial X^2 \partial Y} + \frac{\partial^3}{\partial X^2 \partial Y} \frac{\partial}{\partial Y} \tag{26}$$
$$\tilde{\mathcal{L}}_3(\ ) = \frac{\partial^3}{\partial X^3} \frac{\partial}{\partial X} + \frac{\partial}{\partial X} \frac{\partial^3}{\partial X^3} + \beta^4 \frac{\partial^3}{\partial Y^3} \frac{\partial}{\partial Y} + \beta^4 \frac{\partial}{\partial Y} \frac{\partial^3}{\partial Y^3} + 2 \frac{\partial^2}{\partial X^2} \frac{\partial^2}{\partial X^2} + 2\beta^4 \frac{\partial^2}{\partial Y^2} \frac{\partial^2}{\partial Y^2}$$
$$\tilde{\mathcal{L}}_4(\ ) = \frac{\partial^2}{\partial X^2} \frac{\partial^2}{\partial Y^2} + 2 \frac{\partial^2}{\partial X \partial Y} \frac{\partial^2}{\partial X \partial Y} + \frac{\partial^2}{\partial Y^2} \frac{\partial^2}{\partial X^2} + \frac{\partial^3}{\partial X^2 \partial Y} \frac{\partial}{\partial Y} + \frac{\partial}{\partial Y} \frac{\partial^3}{\partial X^2 \partial Y} + \frac{\partial}{\partial X} \frac{\partial^3}{\partial X \partial Y^2} + \frac{\partial^3}{\partial X \partial Y^2} \frac{\partial}{\partial X}$$

the dimensionless form of the size-dependent nonlinear governing differential equations can be obtained as follow

$$\in^2 \mathcal{L}_{11}(W) + \in^2 2\bar{\tau} \mathcal{L}_{12}(W) - \frac{\partial^2 F}{\partial X^2} = \beta^2 \tilde{\mathcal{L}}_1 (W + W^*, F) + \in^{3/2} \frac{4}{3} 3^{1/4} \mathcal{P}_q \tag{27-a}$$

$$\mathcal{L}_{21}(F) + 2\bar{\tau} \mathcal{L}_{22}(W) + \frac{\partial^2 W}{\partial X^2} = -\frac{\beta^2}{2} \tilde{\mathcal{L}}_1 (W + 2W^*, W) - \bar{\tau} \vartheta_1 \beta^2 \tilde{\mathcal{L}}_2 (W + 2W^*, W) + \bar{\tau} \vartheta_2 \tilde{\mathcal{L}}_3 (W + 2W^*, W) + \frac{\bar{\tau} \vartheta_3 \beta^2}{2} \tilde{\mathcal{L}}_4 (W + 2W^*, W) \tag{27-b}$$

where

$$\vartheta_1 = \frac{a_{11}^*}{(a_{11}^*)^2 - (a_{12}^*)^2} \quad , \quad \vartheta_2 = \frac{a_{12}^*}{(a_{11}^*)^2 - (a_{12}^*)^2}$$
$$\vartheta_3 = \frac{1}{a_{55}^*} \quad , \quad \vartheta_4 = d_{11}^* - e_{11}^* \quad , \quad \vartheta_5 = d_{12}^* + d_{55}^* - e_{11}^* \tag{28}$$

In addition, the boundary conditions in dimensionless form will be at X=0, π

For clamped edge supports: W=0, $\partial W/\partial X$=0

Also, one will have

$$\frac{1}{2\pi} \int_0^{2\pi} \beta^2 \frac{\partial^2 F}{\partial Y^2} dY + \frac{2}{3} 3^{1/4} \in^{3/2} \mathcal{P}_q = 0 = 0 \tag{29}$$

and the closed condition becomes

$$\int_0^{2\pi}\begin{pmatrix} -\vartheta_2\dfrac{\partial^2 F}{\partial Y^2}+\vartheta_1\dfrac{\partial^2 F}{\partial X^2}+\left(1-2\bar{\tau}\vartheta_1\right)\left(W+W^*\right) \\ -\bar{\tau}\vartheta_2\left(\dfrac{\partial\left(W+W^*\right)}{\partial X}\right)^2+\left(1-2\bar{\tau}\vartheta_1\right)\left(\dfrac{\partial\left(W+W^*\right)}{\partial Y}\right)^2 \\ +\left(\vartheta_6\left(\vartheta_1-\vartheta_2\right)\mathcal{V}-2\bar{\tau}\vartheta_7\left(\vartheta_1-\vartheta_2\right)\right)\epsilon \end{pmatrix} dY=0 \quad (30)$$

Moreover, the unit end shortening of nanoshell can be expressed as

$$\delta_q=-\frac{3^{3/4}}{8\pi^2\varepsilon^{3/2}}\int_0^{2\pi}\int_0^{2\pi}\begin{pmatrix} \vartheta_1\beta^2\dfrac{\partial^2 F}{\partial Y^2}-\vartheta_2\dfrac{\partial^2 F}{\partial X^2} \\ +2\bar{\tau}\vartheta_2\left(W+W^*\right)-\dfrac{1}{2}\left(1-2\bar{\tau}\vartheta_1\right)\left(\dfrac{\partial\left(W+W^*\right)}{\partial X}\right)^2 \\ -\bar{\tau}\vartheta_2\beta^2\left(\dfrac{\partial\left(W+W^*\right)}{\partial Y}\right)^2+\left(\vartheta_6\left(\vartheta_1-\vartheta_2\right)\mathcal{V}-2\bar{\tau}\vartheta_7\left(\vartheta_1-\vartheta_2\right)\right)\phi \end{pmatrix} dXdY \quad (31)$$

in which $\vartheta_6=d_{31}R(a_{11}^*+a_{12}^*)/h^2$, $\vartheta_7=R/h$.

3- 2- Singular Perturbation Technique

The important parameter ϵ was introduced in the preceding section. For a shell-type structure, it has been practically indicated that the value of ϵ is always $\epsilon << 1$. So, Eqs. (27) can be considered as boundary layer type equations [54-56] incorporating the both nonlinear prebuckling deformations and large postbuckling deflections in addition to the surface free energy effects. Now, by assuming ϵ as a small perturbation parameter, a two-stepped singular perturbation technique can utilized in which, ϵ is put as the first perturbation parameter. This efficient solution methodology has been successfully applied to the nonlinear analyses of cylindrical shells at macroscale [57-62]. Based on this technique, the independent variables are expressed as the summation of the regular and boundary layer solutions as follow

$$W=\bar{W}\left(X,Y,\epsilon\right)+\tilde{W}\left(X,Y,\epsilon,\xi\right)+\hat{W}\left(X,Y,\epsilon,\varsigma\right) \quad (32\text{-a})$$

$$F=\bar{F}\left(X,Y,\epsilon\right)+\tilde{F}\left(X,Y,\epsilon,\xi\right)+\hat{F}\left(X,Y,\epsilon,\varsigma\right) \quad (32\text{-b})$$

where $\bar{W}(X,Y,\epsilon)$, $\bar{F}(X,Y,\epsilon)$ denote regular solutions of the nanoshell, $\tilde{W}(X,Y,\epsilon,\xi)$, $\tilde{F}(X,Y,\epsilon,\xi)$ and $\hat{W}(X,Y,\epsilon,\varsigma)$, $\hat{F}(X,Y,\epsilon,\varsigma)$ are the boundary layer solutions corresponding to X=0 and X=π, respectively. These solutions are defined in the forms of perturbation expansions as below

$$\begin{aligned} \bar{W}\left(X,Y,\epsilon\right)&=\sum_{i=0}\epsilon^{i/2}\bar{W}_{i/2}\left(X,Y\right) \\ \bar{F}\left(X,Y,\epsilon\right)&=\sum_{i=0}\epsilon^{i/2}\bar{F}_{i/2}\left(X,Y\right) \\ \tilde{W}\left(X,Y,\epsilon,\xi\right)&=\sum_{i=0}\epsilon^{i/2+1}\tilde{W}_{i/2+1}\left(X,Y,\xi\right) \\ \tilde{F}\left(X,Y,\epsilon,\xi\right)&=\sum_{i=0}\epsilon^{i/2+2}\tilde{F}_{i/2+2}\left(X,Y,\xi\right) \\ \hat{W}\left(X,Y,\epsilon,\varsigma\right)&=\sum_{i=0}\epsilon^{i/2+1}\hat{W}_{i/2+1}\left(X,Y,\varsigma\right) \\ \hat{F}\left(X,Y,\epsilon,\varsigma\right)&=\sum_{i=0}\epsilon^{i/2+2}\hat{F}_{i/2+2}\left(X,Y,\varsigma\right) \end{aligned} \quad (33)$$

in which ξ and ς represent the boundary layer variables which are equal to

$$\xi=\frac{X}{\sqrt{\epsilon}} \quad , \quad \varsigma=\frac{\pi-X}{\sqrt{\epsilon}} \quad (34)$$

In addition, it is assumed that

$$\epsilon^{3/2}\frac{4}{3}3^{1/4}q=\sum_{i=0}\epsilon^i\,\mathcal{Q}_i \quad (35)$$

Through substitution Eqs. (32) and (33) into the size-dependent nonlinear governing differential equations (Eq. (27)) and collecting the expressions with the same order of ϵ, the sets of perturbation equations will be derived corresponding to the both regular and boundary layer solutions which are given in Appendix A. After that, it is assumed that $\bar{W}_0(X,Y)=A_{00}^{(0)}$, $\bar{W}_{1/2}(X,Y)=\bar{W}_1(X,Y)=0$ and $\bar{W}_{3/2}(X,Y)=A_{00}^{(3/2)}$ in addition to $\bar{F}_0(X,Y)=-B_{00}^{(0)}(\beta^2X^2+Y^2/2)$, $\bar{F}_{1/2}(X,Y)=\bar{F}_{3/2}(X,Y)=0$, and $\bar{F}_1(X,Y)=-B_{00}^{(1)}(\beta^2X^2+Y^2/2)$. Additionally, the initial buckling mode and the initial geometric imperfection of the nanoshell is assumed in the flowing form

$$\bar{W}_2\left(X,Y\right)=\mathcal{A}_{00}^{(2)}+\mathcal{A}_{11}^{(2)}\sin\left(mX\right)\sin\left(nY\right) \quad (36\text{-a})$$

$$\begin{aligned} W^*\left(X,Y,\epsilon\right)&=\epsilon^2\,\mathcal{A}_{11}^*\sin\left(mX\right)\cos\left(nY\right) \\ &=\epsilon^2\,\ell\mathcal{A}_{11}^{(2)}\sin\left(mX\right)\cos\left(nY\right) \end{aligned} \quad (36\text{-b})$$

in which $l=A_{11}^*/A_{11}^{(2)}$ represents the imperfection parameter. By inserting Eq. (36) in the sets of perturbation equations, the coefficients of $\bar{W}_i(X,Y)$ and $\bar{F}_i(X,Y)$ can be extracted step by step, all of which are in terms of $A_{11}^{(2)}$. The obtained asymptotic solutions corresponding to clamped edge supports are given in Appendix A.

Now, with respect to the given boundary conditions, Eq. (29), closed conditions Eq. (30), and based upon the unit end shortening Eq. (31), the formulations of the postbuckling equilibrium paths can be derived as below

$$\mathcal{P}_q=\frac{1}{2}3^{3/4}\,\epsilon^{-3/2}\left\{\mathcal{P}_q^{(0)}+\mathcal{P}_q^{(2)}\left(A_{11}^{(2)}\epsilon^2\right)^2+\ldots\right\} \quad (37)$$

and

$$\delta_q=\delta_q^{(0)}-\delta_q^E+\delta_q^{(2)}\left(A_{11}^{(2)}\epsilon^2\right)^2+\ldots \quad (38)$$

where $P_q^{(0)}$, $P_q^{(2)}$, $\delta_q^{(0)}$, $\delta_q^{(2)}$, and δ_q^{E} are defined in Appendix A. In the second step of the solution methodology, the maximum dimensionless deflection of the nanoshell $A_{11}^{(2)}\epsilon$ is now considered as the second perturbation parameter which in contrast to the first small perturbation parameter ϵ, it may be large. If it is assumed that the maximum deflection occurs at the dimensionless point of $(X,Y)=(\pi/2m,\pi/2n)$, the second perturbation parameter can be obtained as

$$\mathcal{A}_{11}^{(2)}\epsilon=\mathcal{W}_m+\mathcal{S}_1\mathcal{W}_m^2+\ldots \quad (39)$$

in which W_m stands for the maximum dimensionless deflection of the nanoshell as below

$$\mathcal{W}_m = \in \frac{w_m}{h} + \mathcal{S}_2 \tag{40}$$

where the symbols S_1 and S_2 are given in Appendix A.

4- Results and Discussion

In this section, the postbuckling equilibrium paths of piezoelectric cylindrical nanoshells subjected to combination of hydrostatic pressure and electric field are presented including surface free energy effects and corresponding to the both perfect and imperfect nanoshells. . The material properties of nanoshell are tabulated in Table 1 corresponding to PZT-5H piezoelectric material. Also, in all of the preceding numerical results, it is assumed that the edge supports of nanoshells are clamped and R/h=50, L^2/Rh=200.

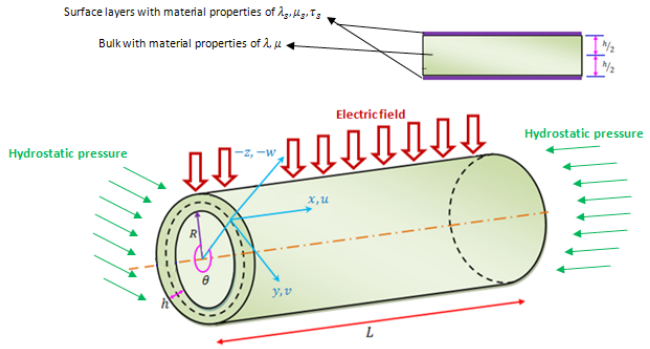

Fig. 1. Schematic view of a piezoelectric cylindrical nanoshell and its surface layers, subjected to hydrostatic pressure and electric field

At first, the validity as well as the accuracy of the present solution methodology is checked. Because in accordance with authors' knowledge, there is no investigation available in the published literature in which the buckling or postbuckling behavior of piezoelectric nanoshells is investigated in the presence of surface stress effects, by ignoring the nonlinear and surface elasticity terms, the critical buckling load of a cylindrical shell at usual scale subjected to lateral pressure is calculated based on the present solution procedure and is compared with that of Mirfakhraei and Redekop [66] using differential quadrature numerical method. In Table 2, the critical buckling pressures of cylindrical shells with clamped edge supports obtained by the two different methods are compared corresponding to the same material and geometric properties. A very good agreement is found which confirms the validity of the current analysis.

Fig. 2 depicts the dimensionless postbuckling load-deflection curves of perfect and imperfect piezoelectric nanoshells with various thicknesses obtained by the classical and non-classical shell models. It is revealed that by increasing the value of shell thickness, the surface free energy effects diminish and the non-classical postbuckling curve shifts to the classical one. Moreover, it can be seen that through moving to the deeper postbuckling regime, the postbuckling curves corresponding to various shell thicknesses tend to each other which means that by increasing the deflection in postbuckling domain, the effects of surface free energy decrease. These anticipations are the same for the both perfect and imperfect nanoshells.

Illustrated in Fig. 3 are the classical and non-classical dimensionless load-shortening equilibrium curves of perfect

Table 1. Material properties of a cylindrical nanoshell made of Silicon [63-65]

λ (Pa)	31×10^9
μ (Pa)	35.5×10^9
ν	0.3
μ_s (N/m)	2.31
λ_s (N/m)	3.3
τ_s (N/m)	1
d_{31} (m/V)	-2.65×10^{-10}

Table 2. Comparison of the critical buckling pressures of isotropic cylindrical shells with clamped edge supports subjected to lateral pressure (ν=0.3, E=200 GPa)

L/R	R/h	Present work (Pa)	Ref. [66] (Pa)
2	300	84991.09	85860
	3000	275.82	276.5
5	300	32897.22	32954
	3000	108.13	109

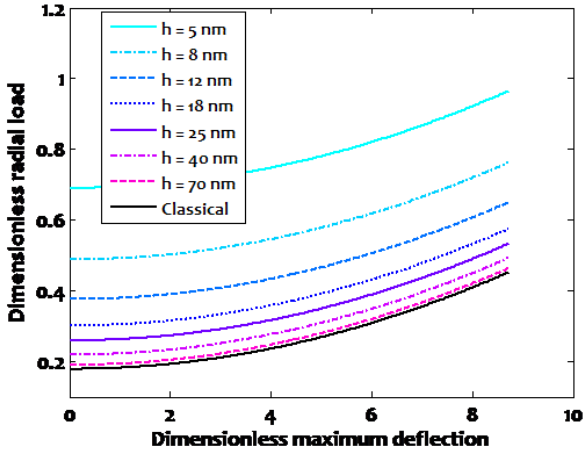

(a)

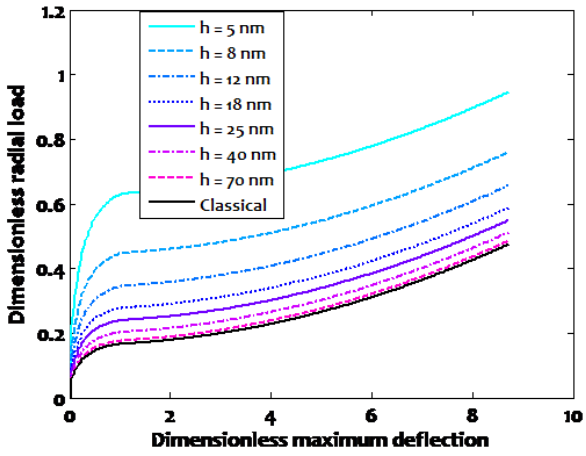

(b)

Fig. 2. Dimensionless postbuckling load-deflection curves of piezoelectric nanoshells with various shell thickness (V=0); (a) W^*=0, (b) W^*=0.1

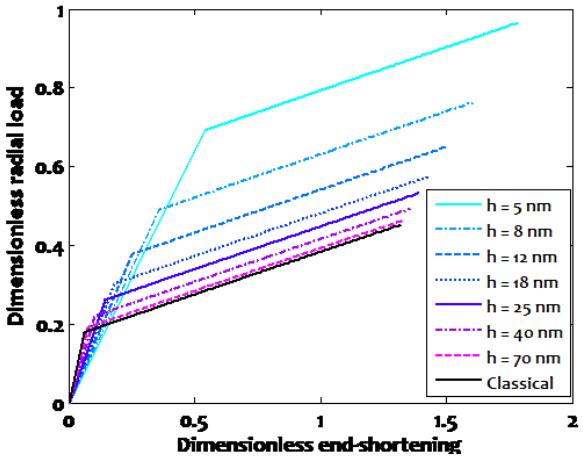

(a)

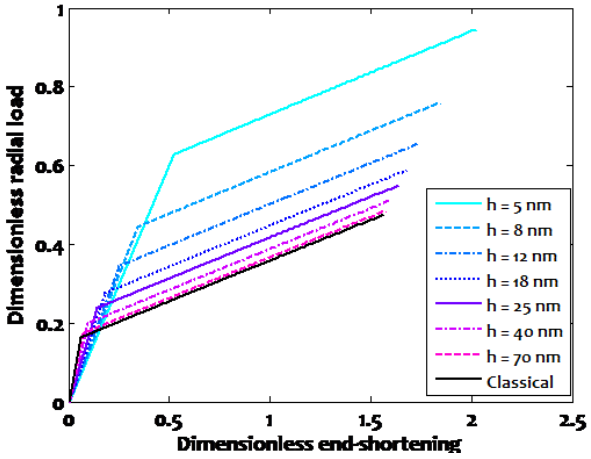

(b)

Fig. 3. Dimensionless postbuckling load-shortening curves of piezoelectric nanoshells with various shell thickness (V=0); (a) W^*=0, (b) W^*=0.1

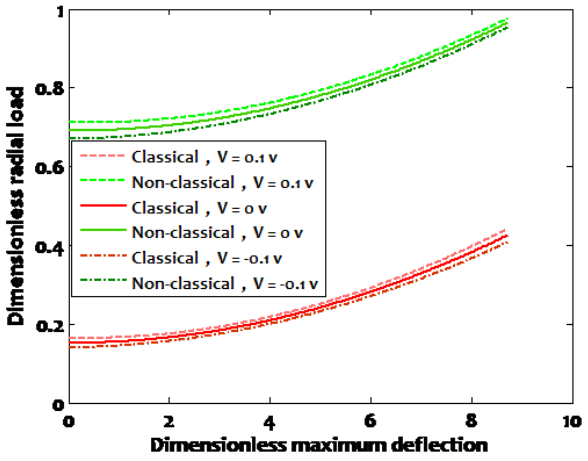

(a)

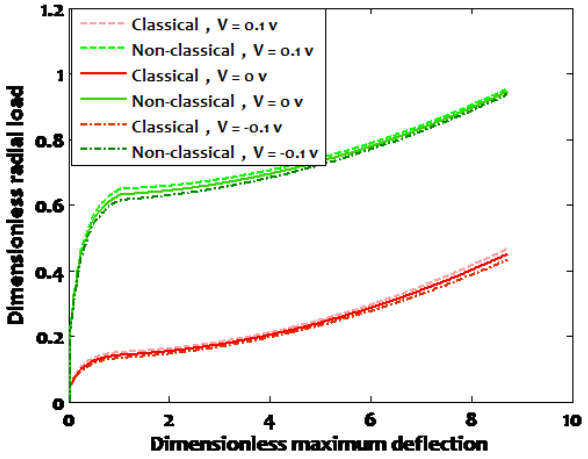

(b)

Fig. 4. Influence of applied electrical load on the postbuckling load-deflection curves of piezoelectric nanoshell corresponding to various values of applied voltage (h=5 nm); (a) W^*=0, (b) W^*=0.1

and imperfect piezoelectric nanoshells corresponding to different shell thicknesses. It is observed that for a piezoelectric cylindrical nanoshell made of PZT-5H, surface free energy effects cause to increase the both critical buckling pressure and critical end-shortening in such a way that the slope of prebuckling part of load-shortening equilibrium curve increases. This observation is more considerable for piezoelectric nanoshell with lower value of shell thickness. This pattern is similar for nanoshells with and without initial geometric imperfection.

Figs. 4 and 5 show, respectively, the dimensionless load-deflection and load-shortening equilibrium paths obtained by the classical and non-classical shell models for piezoelectric nanoshells subjected to various voltages. It is found that for the both classical and non-classical shell models, by applying an electric field with positive voltage, the both critical buckling pressure and critical end-shortening of nanoshell increase while an electric field with negative voltage has an opposite influence. Also, it can be seen that by taking surface free energy effects into account, the influence of electrical load on the postbuckling behavior of nanoshell increases. Additionally, it is revealed that in contrast to the classical shell model, by moving to deeper postbuckling regime of the non-classical load-deflection equilibrium paths, the influence of electric field decreases.

Plotted in Fig. 6 are the dimensionless load-deflection and load-shortening equilibrium paths of perfect and imperfect cylindrical nanoshells corresponding to various surface elastic constants. It can be observed that surface free energy effects may cause to increase or decrease the stiffness of piezoelectric nanoshell which depends on the sign of surface elastic constants. It is seen that the size effect corresponding to positive surface elastic constants leads to increase the critical buckling load, while the size effect corresponding to negative surface elastic constants cause to decrease it.

5- Concluding

The purpose of the present investigation was to analyze the size-dependent buckling and postbuckling behavior of piezoelectric cylindrical nanoshells subjected to radial compression combined with electric load in the presence of surface free energy effects. To this end, the Gurtin-Murdoch elasticity theory was implemented into the classical shell

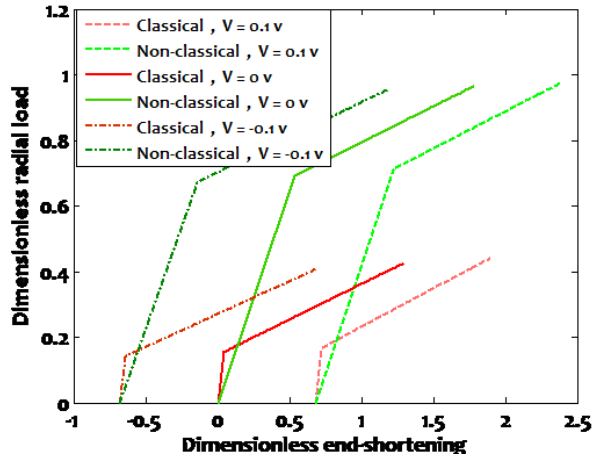

(a)

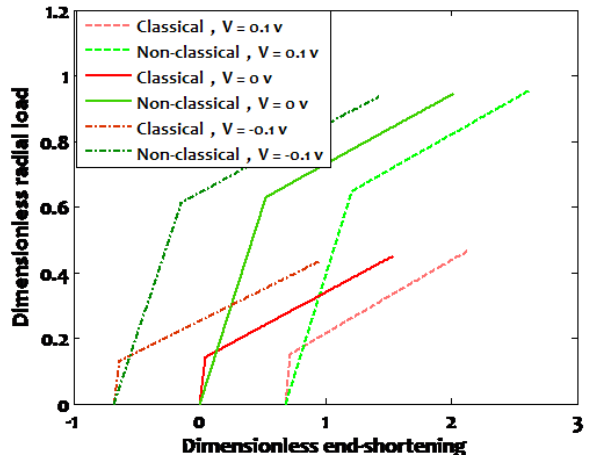

(b)

Fig. 5. Influence of applied electrical load on the postbuckling load-shortening curves of piezoelectric nanoshell corresponding to various values of applied voltage (h=5 nm); (a) W^*=0, (b) W^*=0.1

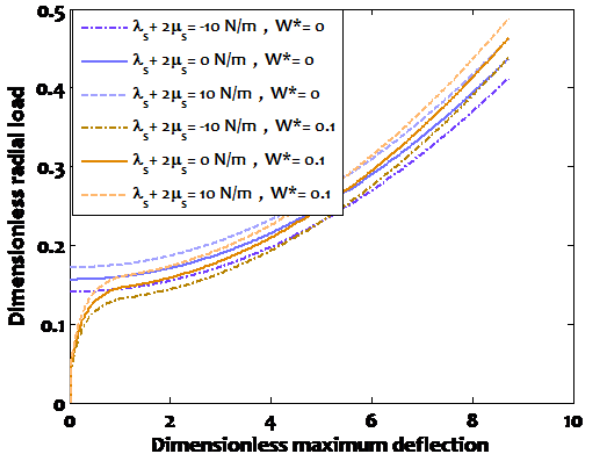

(a)

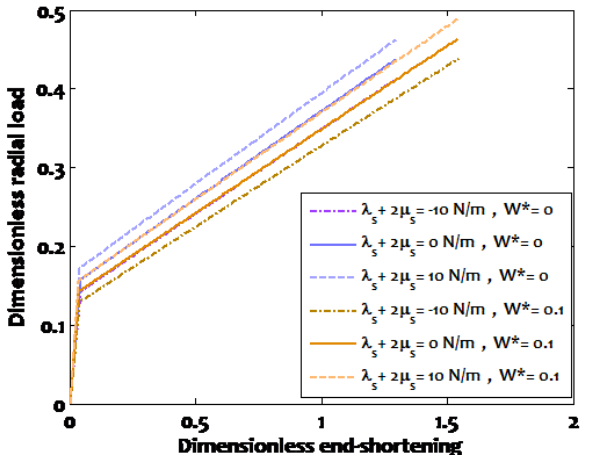

(b)

Fig. 6. Influence of surface elastic constants on the buckling and postbuckling behavior of perfect and imperfect piezoelectric nanoshell subjected to axial compression (h=5 nm,V=0)

theory to develop an efficient non-classical shell model. After that, a boundary layer theory in conjunction with a two-stepped singular perturbation technique was employed to obtain the size-dependent critical buckling pressures and associated postbuckling equilibrium paths corresponding to various shell thicknesses, applied voltages and surface elastic constants.

It was demonstrated that by increasing the value of shell thickness, the surface free energy effects diminish and the non-classical postbuckling curve shifts to the classical one. Furthermore, It was indicated that for a piezoelectric cylindrical nanoshell made of PZT-5H, surface free energy effects cause to increase the both critical buckling pressure and critical end-shortening in such a way that the slope of prebuckling part of load-shortening equilibrium curve increases. In addition, it was seen that by increasing the deflection in postbuckling domain, the effects of surface free energy decrease. Also, it was found that for the both classical and non-classical shell models, by applying an electric field with positive voltage, the both critical buckling pressure and critical end-shortening of nanoshell increase while an electric field with negative voltage has an opposite influence. Additionally, it was seen that by taking surface free energy effects into account, the influence of electrical load on the postbuckling behavior of nanoshell increases. It was observed that surface free energy effects may cause to increase or decrease the stiffness of piezoelectric nanoshell which depends on the sign of surface elastic constants.

Appendix A

The sets of perturbation equations for the regular solution are:

$$O(\epsilon^0):\begin{cases} -\dfrac{\partial^2 \bar{F}_0}{\partial X^2} = \beta^2 \tilde{L}_1(\bar{W}_0, \bar{F}_0) + Q_0 \\ \mathcal{L}_{21}(\bar{F}_0) + 2\bar{\tau}\mathcal{L}_{22}(\bar{W}_0) + \dfrac{\partial^2 \bar{W}_0}{\partial X^2} = -\dfrac{\beta^2}{2}\tilde{L}_1(\bar{W}_0, \bar{W}_0) - \bar{\tau}\vartheta_1\beta^2\tilde{L}_2(\bar{W}_0, \bar{W}_0) + \bar{\tau}\vartheta_2\tilde{L}_3(\bar{W}_0, \bar{W}_0) \\ \qquad + \dfrac{\bar{\tau}\vartheta_3\beta^2}{2}\tilde{L}_4(\bar{W}_0, \bar{W}_0) \end{cases}$$

$$O(\epsilon^{1/2}):\begin{cases} -\dfrac{\partial^2 \bar{F}_{1/2}}{\partial X^2} = \beta^2 \tilde{L}_1(\bar{W}_{1/2}, \bar{F}_0) + \beta^2 \tilde{L}_1(\bar{W}_0, \bar{F}_{1/2}) \\ \mathcal{L}_{21}(\bar{F}_{1/2}) + 2\bar{\tau}\mathcal{L}_{22}(\bar{W}_{1/2}) + \dfrac{\partial^2 \bar{W}_{1/2}}{\partial X^2} = -\dfrac{\beta^2}{2}\tilde{L}_1(\bar{W}_0, \bar{W}_{1/2}) - \bar{\tau}\vartheta_1\beta^2\tilde{L}_2(\bar{W}_0, \bar{W}_{1/2}) \\ \qquad + \bar{\tau}\vartheta_2\tilde{L}_3(\bar{W}_0, \bar{W}_{1/2}) + \dfrac{\bar{\tau}\vartheta_3\beta^2}{2}\tilde{L}_4(\bar{W}_0, \bar{W}_{1/2}) \end{cases}$$

$$O(\epsilon^1):\begin{cases}-\dfrac{\partial^2\bar{F}_1}{\partial X^2}=\beta^2\tilde{L}_1(\bar{W}_{1/2},\bar{F}_{1/2})+\beta^2\tilde{L}_1(\bar{W}_1,\bar{F}_0)+\beta^2\tilde{L}_1(\bar{W}_0,\bar{F}_1)+Q_1\\ \mathcal{L}_{21}(\bar{F}_1)+2\bar{\tau}\mathcal{L}_{22}(\bar{W}_1)+\dfrac{\partial^2\bar{W}_1}{\partial X^2}=-\dfrac{\beta^2}{2}\tilde{L}_1(\bar{W}_0,\bar{W}_1)-\dfrac{\beta^2}{2}\tilde{L}_1(\bar{W}_{1/2},\bar{W}_{1/2})-\bar{\tau}\vartheta_1\beta^2\tilde{L}_2(\bar{W}_0,\bar{W}_1)\\ \quad-\bar{\tau}\vartheta_1\beta^2\tilde{L}_2(\bar{W}_{1/2},\bar{W}_{1/2})+\bar{\tau}\vartheta_2\tilde{L}_3(\bar{W}_0,\bar{W}_1)+\bar{\tau}\vartheta_2\tilde{L}_3(\bar{W}_{1/2},\bar{W}_{1/2})+\dfrac{\bar{\tau}\vartheta_3\beta^2}{2}\tilde{L}_4(\bar{W}_0,\bar{W}_1)\\ \quad+\dfrac{\bar{\tau}\vartheta_3\beta^2}{2}\tilde{L}_4(\bar{W}_{1/2},\bar{W}_{1/2})\end{cases}$$

$$O(\epsilon^{3/2}):\begin{cases}-\dfrac{\partial^2\bar{F}_{3/2}}{\partial X^2}=\beta^2\tilde{L}_1(\bar{W}_0,\bar{F}_{3/2})+\beta^2\tilde{L}_1(\bar{W}_{1/2},\bar{F}_1)+\beta^2\tilde{L}_1(\bar{W}_1,\bar{F}_{1/2})+\beta^2\tilde{L}_1(\bar{W}_{3/2},\bar{F}_0)\\ \mathcal{L}_{21}(\bar{F}_{3/2})+2\bar{\tau}\mathcal{L}_{22}(\bar{W}_{3/2})+\dfrac{\partial^2\bar{W}_{3/2}}{\partial X^2}=-\dfrac{\beta^2}{2}\tilde{L}_1(\bar{W}_0,\bar{W}_{3/2})-\dfrac{\beta^2}{2}\tilde{L}_1(\bar{W}_{1/2},\bar{W}_1)\\ \quad-\bar{\tau}\vartheta_1\beta^2\tilde{L}_2(\bar{W}_0,\bar{W}_{3/2})-\bar{\tau}\vartheta_1\beta^2\tilde{L}_2(\bar{W}_{1/2},\bar{W}_1)+\bar{\tau}\vartheta_2\tilde{L}_3(\bar{W}_0,\bar{W}_{3/2})+\bar{\tau}\vartheta_2\tilde{L}_3(\bar{W}_{1/2},\bar{W}_1)\\ \quad+\dfrac{\bar{\tau}\vartheta_3\beta^2}{2}\tilde{L}_4(\bar{W}_0,\bar{W}_{3/2})+\dfrac{\bar{\tau}\vartheta_3\beta^2}{2}\tilde{L}_4(\bar{W}_{1/2},\bar{W}_1)\end{cases}$$

$$O(\epsilon^2):\begin{cases}\mathcal{L}_{11}(\bar{W}_0)+2\bar{\tau}\mathcal{L}_{12}(\bar{W}_0)-\dfrac{\partial^2\bar{F}_2}{\partial X^2}=\beta^2\tilde{L}_1(\bar{W}_0,\bar{F}_2)+\beta^2\tilde{L}_1(\bar{W}_{1/2},\bar{F}_{3/2})+\beta^2\tilde{L}_1(\bar{W}_1,\bar{F}_1)\\ \quad+\beta^2\tilde{L}_1(\bar{W}_{3/2},\bar{F}_{1/2})+\beta^2\tilde{L}_1(\bar{W}_2+W^*,\bar{F}_0)+Q_2\\ \mathcal{L}_{21}(\bar{F}_2)+2\bar{\tau}\mathcal{L}_{22}(\bar{W}_2)+\dfrac{\partial^2\bar{W}_2}{\partial X^2}=-\dfrac{\beta^2}{2}\tilde{L}_1(\bar{W}_0,\bar{W}_2)-\dfrac{\beta^2}{2}\tilde{L}_1(\bar{W}_{1/2},\bar{W}_{3/2})-\dfrac{\beta^2}{2}\tilde{L}_1(\bar{W}_1,\bar{W}_1)\\ \quad-\bar{\tau}\vartheta_1\beta^2\tilde{L}_2(\bar{W}_0,\bar{W}_2+2W^*)-\bar{\tau}\vartheta_1\beta^2\tilde{L}_2(\bar{W}_{1/2},\bar{W}_{3/2})-\bar{\tau}\vartheta_1\beta^2\tilde{L}_2(\bar{W}_1,\bar{W}_1)\\ \quad+\bar{\tau}\vartheta_2\tilde{L}_3(\bar{W}_0,\bar{W}_2+2W^*)+\bar{\tau}\vartheta_2\tilde{L}_3(\bar{W}_{1/2},\bar{W}_{3/2})+\bar{\tau}\vartheta_2\tilde{L}_3(\bar{W}_1,\bar{W}_1)\\ \quad+\dfrac{\bar{\tau}\vartheta_3\beta^2}{2}\tilde{L}_4(\bar{W}_0,\bar{W}_2)+\dfrac{\bar{\tau}\vartheta_3\beta^2}{2}\tilde{L}_4(\bar{W}_{1/2},\bar{W}_{3/2})+\dfrac{\bar{\tau}\vartheta_3\beta^2}{2}\tilde{L}_4(\bar{W}_1,\bar{W}_1)\end{cases}$$

$$O(\epsilon^{5/2}):\begin{cases}\mathcal{L}_{11}(\bar{W}_{1/2})+2\bar{\tau}\mathcal{L}_{12}(\bar{W}_{1/2})-\dfrac{\partial^2\bar{F}_{5/2}}{\partial X^2}=\beta^2\tilde{L}_1(\bar{W}_0,\bar{F}_{5/2})+\beta^2\tilde{L}_1(\bar{W}_{1/2},\bar{F}_2)+\beta^2\tilde{L}_1(\bar{W}_1,\bar{F}_{3/2})\\ \quad+\beta^2\tilde{L}_1(\bar{W}_{3/2},\bar{F}_1)+\beta^2\tilde{L}_1(\bar{W}_2+W^*,\bar{F}_{1/2})+\beta^2\tilde{L}_1(\bar{W}_{5/2},\bar{F}_0)\\ \mathcal{L}_{21}(\bar{F}_{5/2})+2\bar{\tau}\mathcal{L}_{22}(\bar{W}_{5/2})+\dfrac{\partial^2\bar{W}_{5/2}}{\partial X^2}=-\dfrac{\beta^2}{2}\tilde{L}_1(\bar{W}_0,\bar{W}_{5/2})-\dfrac{\beta^2}{2}\tilde{L}_1(\bar{W}_{1/2},\bar{W}_2+2W^*)\\ \quad-\dfrac{\beta^2}{2}\tilde{L}_1(\bar{W}_1,\bar{W}_{3/2})-\bar{\tau}\vartheta_1\beta^2\tilde{L}_2(\bar{W}_0,\bar{W}_{5/2})-\bar{\tau}\vartheta_1\beta^2\tilde{L}_2(\bar{W}_{1/2},\bar{W}_2+2W^*)\\ \quad-\bar{\tau}\vartheta_1\beta^2\tilde{L}_2(\bar{W}_1,\bar{W}_{3/2})+\bar{\tau}\vartheta_2\tilde{L}_3(\bar{W}_0,\bar{W}_{5/2})+\bar{\tau}\vartheta_2\tilde{L}_3(\bar{W}_{1/2},\bar{W}_2+2W^*)+\bar{\tau}\vartheta_2\tilde{L}_3(\bar{W}_1,\bar{W}_{3/2})\\ \quad+\dfrac{\bar{\tau}\vartheta_3\beta^2}{2}\tilde{L}_4(\bar{W}_{1/2},\bar{W}_2+2W^*)+\dfrac{\bar{\tau}\vartheta_3\beta^2}{2}\tilde{L}_4(\bar{W}_1,\bar{W}_{3/2})+\dfrac{\bar{\tau}\vartheta_3\beta^2}{2}\tilde{L}_4(\bar{W}_0,\bar{W}_{5/2})\end{cases}$$

$$O(\epsilon^3):\begin{cases}\mathcal{L}_{11}(\bar{W}_1)+2\bar{\tau}\mathcal{L}_{12}(\bar{W}_1)-\dfrac{\partial^2\bar{F}_3}{\partial X^2}=\beta^2\tilde{L}_1(\bar{W}_0,\bar{F}_3)+\beta^2\tilde{L}_1(\bar{W}_{1/2},\bar{F}_{5/2})+\beta^2\tilde{L}_1(\bar{W}_1,\bar{F}_2)\\ \quad+\beta^2\tilde{L}_1(\bar{W}_{3/2},\bar{F}_{3/2})+\beta^2\tilde{L}_1(\bar{W}_2+W^*,\bar{F}_1)+\beta^2\tilde{L}_1(\bar{W}_{5/2},\bar{F}_{1/2})+\beta^2\tilde{L}_1(\bar{W}_3,\bar{F}_0)+Q_3\\ \mathcal{L}_{21}(\bar{F}_3)+2\bar{\tau}\mathcal{L}_{22}(\bar{W}_3)+\dfrac{\partial^2\bar{W}_3}{\partial X^2}=-\dfrac{\beta^2}{2}\tilde{L}_1(\bar{W}_0,\bar{W}_3)-\dfrac{\beta^2}{2}\tilde{L}_1(\bar{W}_{1/2},\bar{W}_{5/2})-\dfrac{\beta^2}{2}\tilde{L}_1(\bar{W}_1,\bar{W}_2+2W^*)\\ \quad-\dfrac{\beta^2}{2}\tilde{L}_1(\bar{W}_{3/2},\bar{W}_{3/2})-\bar{\tau}\vartheta_1\beta^2\tilde{L}_2(\bar{W}_0,\bar{W}_3)-\bar{\tau}\vartheta_1\beta^2\tilde{L}_2(\bar{W}_{1/2},\bar{W}_{5/2})\\ \quad-\bar{\tau}\vartheta_1\beta^2\tilde{L}_2(\bar{W}_1,\bar{W}_2+2W^*)-\bar{\tau}\vartheta_1\beta^2\tilde{L}_2(\bar{W}_{3/2},\bar{W}_{3/2})+\bar{\tau}\vartheta_2\tilde{L}_3(\bar{W}_0,\bar{W}_3)+\bar{\tau}\vartheta_2\tilde{L}_3(\bar{W}_{1/2},\bar{W}_{5/2})\\ \quad+\bar{\tau}\vartheta_2\tilde{L}_3(\bar{W}_1,\bar{W}_2+2W^*)+\bar{\tau}\vartheta_2\tilde{L}_3(\bar{W}_1,\bar{W}_2+2W^*)+\bar{\tau}\vartheta_2\tilde{L}_3(\bar{W}_{3/2},\bar{W}_{3/2})\\ \quad+\dfrac{\bar{\tau}\vartheta_3\beta^2}{2}\tilde{L}_4(\bar{W}_0,\bar{W}_3)+\dfrac{\bar{\tau}\vartheta_3\beta^2}{2}\tilde{L}_4(\bar{W}_{1/2},\bar{W}_{5/2})+\dfrac{\bar{\tau}\vartheta_3\beta^2}{2}\tilde{L}_4(\bar{W}_1,\bar{W}_2+2W^*)\\ \quad+\dfrac{\bar{\tau}\vartheta_3\beta^2}{2}\tilde{L}_4(\bar{W}_{3/2},\bar{W}_{3/2})\end{cases}$$

$$O(\epsilon^{7/2}):\begin{cases}\mathcal{L}_{11}(\bar{W}_{3/2})+2\bar{\tau}\mathcal{L}_{12}(\bar{W}_{3/2})-\dfrac{\partial^2\bar{F}_{7/2}}{\partial X^2}=\beta^2\tilde{L}_1(\bar{W}_0,\bar{F}_{7/2})+\beta^2\tilde{L}_1(\bar{W}_{1/2},\bar{F}_3)+\beta^2\tilde{L}_1(\bar{W}_1,\bar{F}_{5/2})\\ \quad+\beta^2\tilde{L}_1(\bar{W}_{3/2},\bar{F}_2)+\beta^2\tilde{L}_1(\bar{W}_2+W^*,\bar{F}_{3/2})+\beta^2\tilde{L}_1(\bar{W}_{5/2},\bar{F}_1)+\beta^2\tilde{L}_1(\bar{W}_3,\bar{F}_{1/2})\\ \quad+\beta^2\tilde{L}_1(\bar{W}_{7/2},\bar{F}_0)\\ \mathcal{L}_{21}(\bar{F}_{7/2})+2\bar{\tau}\mathcal{L}_{22}(\bar{W}_{7/2})+\dfrac{\partial^2\bar{W}_{7/2}}{\partial X^2}=-\dfrac{\beta^2}{2}\tilde{L}_1(\bar{W}_0,\bar{W}_{7/2})-\dfrac{\beta^2}{2}\tilde{L}_1(\bar{W}_{1/2},\bar{W}_3)\\ \quad-\dfrac{\beta^2}{2}\tilde{L}_1(\bar{W}_1,\bar{W}_{5/2})-\dfrac{\beta^2}{2}\tilde{L}_1(\bar{W}_{3/2},\bar{W}_2+2W^*)-\bar{\tau}\vartheta_1\beta^2\tilde{L}_2(\bar{W}_0,\bar{W}_{7/2})\\ \quad-\bar{\tau}\vartheta_1\beta^2\tilde{L}_2(\bar{W}_{1/2},\bar{W}_3)-\bar{\tau}\vartheta_1\beta^2\tilde{L}_2(\bar{W}_1,\bar{W}_{5/2})-\bar{\tau}\vartheta_1\beta^2\tilde{L}_2(\bar{W}_{3/2},\bar{W}_2+2W^*)\\ \quad+\bar{\tau}\vartheta_2\tilde{L}_3(\bar{W}_0,\bar{W}_{7/2})+\bar{\tau}\vartheta_2\tilde{L}_3(\bar{W}_{1/2},\bar{W}_3)+\bar{\tau}\vartheta_2\tilde{L}_3(\bar{W}_1,\bar{W}_{5/2})\\ \quad+\bar{\tau}\vartheta_2\tilde{L}_3(\bar{W}_{3/2},\bar{W}_2+2W^*)+\dfrac{\bar{\tau}\vartheta_3\beta^2}{2}\tilde{L}_4(\bar{W}_0,\bar{W}_{7/2})+\dfrac{\bar{\tau}\vartheta_3\beta^2}{2}\tilde{L}_4(\bar{W}_{1/2},\bar{W}_3)\\ \quad+\dfrac{\bar{\tau}\vartheta_3\beta^2}{2}\tilde{L}_4(\bar{W}_1,\bar{W}_{5/2})+\dfrac{\bar{\tau}\vartheta_3\beta^2}{2}\tilde{L}_4(\bar{W}_{3/2},\bar{W}_2+2W^*)\end{cases}$$

$$O(\epsilon^4):\begin{cases}\mathcal{L}_{11}(\bar{W}_2)+2\bar{\tau}\mathcal{L}_{12}(\bar{W}_2)-\dfrac{\partial^2\bar{F}_4}{\partial X^2}=\beta^2\tilde{L}_1(\bar{W}_0,\bar{F}_4)+\beta^2\tilde{L}_1(\bar{W}_{1/2},\bar{F}_{7/2})+\beta^2\tilde{L}_1(\bar{W}_1,\bar{F}_3)\\ \quad+\beta^2\tilde{L}_1(\bar{W}_{3/2},\bar{F}_{5/2})+\beta^2\tilde{L}_1(\bar{W}_2+W^*,\bar{F}_2)+\beta^2\tilde{L}_1(\bar{W}_{5/2},\bar{F}_{3/2})+\beta^2\tilde{L}_1(\bar{W}_3,\bar{F}_1)\\ \quad+\beta^2\tilde{L}_1(\bar{W}_{7/2},\bar{F}_{1/2})+\beta^2\tilde{L}_1(\bar{W}_4,\bar{F}_0)+Q_4\\ \mathcal{L}_{21}(\bar{F}_4)+2\bar{\tau}\mathcal{L}_{22}(\bar{W}_4)+\dfrac{\partial^2\bar{W}_4}{\partial X^2}=-\dfrac{\beta^2}{2}\tilde{L}_1(\bar{W}_0,\bar{W}_4)-\dfrac{\beta^2}{2}\tilde{L}_1(\bar{W}_{1/2},\bar{W}_{7/2})-\dfrac{\beta^2}{2}\tilde{L}_1(\bar{W}_1,\bar{W}_3)\\ \quad-\dfrac{\beta^2}{2}\tilde{L}_1(\bar{W}_{3/2},\bar{W}_{5/2})-\dfrac{\beta^2}{2}\tilde{L}_1(\bar{W}_2+2W^*,\bar{W}_2)-\bar{\tau}\vartheta_1\beta^2\tilde{L}_2(\bar{W}_0,\bar{W}_4)\\ \quad-\bar{\tau}\vartheta_1\beta^2\tilde{L}_2(\bar{W}_{1/2},\bar{W}_{7/2})-\bar{\tau}\vartheta_1\beta^2\tilde{L}_2(\bar{W}_1,\bar{W}_3)-\bar{\tau}\vartheta_1\beta^2\tilde{L}_2(\bar{W}_{3/2},\bar{W}_{5/2})\\ \quad-\bar{\tau}\vartheta_1\beta^2\tilde{L}_2(\bar{W}_2+2W^*,\bar{W}_2)+\bar{\tau}\vartheta_2\tilde{L}_3(\bar{W}_0,\bar{W}_4)+\bar{\tau}\vartheta_2\tilde{L}_3(\bar{W}_{1/2},\bar{W}_{7/2})+\bar{\tau}\vartheta_2\tilde{L}_3(\bar{W}_1,\bar{W}_3)\\ \quad+\bar{\tau}\vartheta_2\tilde{L}_3(\bar{W}_{3/2},\bar{W}_{5/2})+\bar{\tau}\vartheta_2\tilde{L}_3(\bar{W}_2+2W^*,\bar{W}_2)+\dfrac{\bar{\tau}\vartheta_3\beta^2}{2}\tilde{L}_4(\bar{W}_0,\bar{W}_4)\\ \quad+\dfrac{\bar{\tau}\vartheta_3\beta^2}{2}\tilde{L}_4(\bar{W}_{1/2},\bar{W}_{7/2})+\dfrac{\bar{\tau}\vartheta_3\beta^2}{2}\tilde{L}_4(\bar{W}_1,\bar{W}_3)+\dfrac{\bar{\tau}\vartheta_3\beta^2}{2}\tilde{L}_4(\bar{W}_{3/2},\bar{W}_{5/2})\\ \quad+\dfrac{\bar{\tau}\vartheta_3\beta^2}{2}\tilde{L}_4(\bar{W}_2+2W^*,\bar{W}_2)\end{cases}\tag{A1}$$

The sets of perturbation equations for the boundary layer solutions are:

$$O\left(\in^{5/2}\right):\begin{cases}\mathcal{G}_4\dfrac{\partial^4\tilde{W}_{3/2}}{\partial\xi^4}-\dfrac{\partial^2\tilde{F}_{5/2}}{\partial\xi^2}=0\\ \mathcal{G}_1\dfrac{\partial^4\tilde{F}_{5/2}}{\partial\xi^4}+\left(1-2\bar{\tau}\mathcal{G}_1\right)\dfrac{\partial^2\tilde{W}_{3/2}}{\partial\xi^2}=0\end{cases}$$

$$O\left(\in^3\right):\begin{cases}\mathcal{G}_4\dfrac{\partial^4\tilde{W}_2}{\partial\xi^4}-\dfrac{\partial^2\tilde{F}_3}{\partial\xi^2}=0\\ \mathcal{G}_1\dfrac{\partial^4\tilde{F}_3}{\partial\xi^4}+\left(1-2\bar{\tau}\mathcal{G}_1\right)\dfrac{\partial^2\tilde{W}_2}{\partial\xi^2}=0\end{cases}\tag{A2}$$

$$O\left(\in^{5/2}\right):\begin{cases}\mathcal{G}_4\dfrac{\partial^4\hat{W}_{3/2}}{\partial\varsigma^4}-\dfrac{\partial^2\hat{F}_{5/2}}{\partial\varsigma^2}=0\\ \mathcal{G}_1\dfrac{\partial^4\hat{F}_{5/2}}{\partial\varsigma^4}+\left(1-2\bar{\tau}\mathcal{G}_1\right)\dfrac{\partial^2\hat{W}_{3/2}}{\partial\varsigma^2}=0\end{cases}$$

$$O\left(\in^3\right):\begin{cases}\mathcal{G}_4\dfrac{\partial^4\hat{W}_2}{\partial\varsigma^4}-\dfrac{\partial^2\hat{F}_3}{\partial\varsigma^2}=0\\ \mathcal{G}_1\dfrac{\partial^4\hat{F}_3}{\partial\varsigma^4}+\left(1-2\bar{\tau}\mathcal{G}_1\right)\dfrac{\partial^2\hat{W}_2}{\partial\varsigma^2}=0\end{cases}$$

The obtained asymptotic solution corresponding to clamped edge supports are:

$$\begin{aligned}W=&\mathcal{A}_{00}^{(0)}+\delta^{3/2}\left[\mathcal{A}_{00}^{(3/2)}-\mathcal{A}_{00}^{(3/2)}\left(\sin\left(\frac{\alpha X}{\sqrt{\epsilon}}\right)+\cos\left(\frac{\alpha X}{\sqrt{\epsilon}}\right)\right)e^{-\frac{\alpha X}{\sqrt{\epsilon}}}-\mathcal{A}_{00}^{(3/2)}\left(\sin\left(\frac{\alpha(\pi-X)}{\sqrt{\epsilon}}\right)+\cos\left(\frac{\alpha(\pi-X)}{\sqrt{\epsilon}}\right)\right)e^{-\frac{\alpha(\pi-X)}{\sqrt{\epsilon}}}\right]\\&+\epsilon^2\left[\mathcal{A}_{00}^{(2)}+\mathcal{A}_{11}^{(2)}\sin(mX)\sin(nY)-\mathcal{A}_{00}^{(2)}\left(\sin\left(\frac{\alpha X}{\sqrt{\epsilon}}\right)+\cos\left(\frac{\alpha X}{\sqrt{\epsilon}}\right)\right)e^{-\frac{\alpha X}{\sqrt{\epsilon}}}-\mathcal{A}_{00}^{(2)}\left(\sin\left(\frac{\alpha(\pi-X)}{\sqrt{\epsilon}}\right)+\cos\left(\frac{\alpha(\pi-X)}{\sqrt{\epsilon}}\right)\right)e^{-\frac{\alpha(\pi-X)}{\sqrt{\epsilon}}}\right]\\&+\epsilon^4\left[\mathcal{A}_{00}^{(4)}+\mathcal{A}_{11}^{(4)}\sin(mX)\sin(nY)+\mathcal{A}_{10}^{(4)}\cos(2mX)+\mathcal{A}_{01}^{(4)}\cos(2nY)+\mathcal{A}_{11}^{(4)}\cos(2mX)\cos(2nY)\right]+O(\epsilon^5)\end{aligned}\tag{A3}$$

$$\begin{aligned}F=&-\mathcal{B}_{00}^{(0)}\left(\beta^2X^2+\frac{Y^2}{2}\right)+\epsilon^2\left[-\mathcal{B}_{00}^{(2)}\left(\beta^2X^2+\frac{Y^2}{2}\right)+\mathcal{B}_{11}^{(2)}\sin(mX)\sin(nY)\right]\\&+\epsilon^{5/2}\left[+\mathcal{A}_{00}^{(3/2)}\left(\mathcal{B}_{10}^{(3/2)}\sin\left(\frac{\alpha X}{\sqrt{\epsilon}}\right)+\mathcal{B}_{01}^{(3/2)}\cos\left(\frac{\alpha X}{\sqrt{\epsilon}}\right)\right)e^{-\frac{\alpha X}{\sqrt{\epsilon}}}\right.\\&\left.+\mathcal{A}_{00}^{(3/2)}\left(\mathcal{B}_{10}^{(5/2)}\sin\left(\frac{\alpha(\pi-X)}{\sqrt{\epsilon}}\right)+\mathcal{B}_{01}^{(5/2)}\cos\left(\frac{\alpha(\pi-X)}{\sqrt{\epsilon}}\right)\right)e^{-\frac{\alpha(\pi-X)}{\sqrt{\epsilon}}}\right]\\&+\epsilon^3\left[\mathcal{A}_{00}^{(2)}\left(\mathcal{B}_{10}^{(3)}\sin\left(\frac{\alpha X}{\sqrt{\epsilon}}\right)+\mathcal{B}_{01}^{(3)}\cos\left(\frac{\alpha X}{\sqrt{\epsilon}}\right)\right)e^{-\frac{\alpha X}{\sqrt{\epsilon}}}\right.\\&\left.+\mathcal{A}_{00}^{(2)}\left(\mathcal{B}_{10}^{(3)}\sin\left(\frac{\alpha(\pi-X)}{\sqrt{\epsilon}}\right)+\mathcal{B}_{01}^{(3)}\cos\left(\frac{\alpha(\pi-X)}{\sqrt{\epsilon}}\right)\right)e^{-\frac{\alpha(\pi-X)}{\sqrt{\epsilon}}}\right]\\&+\epsilon^4\left[-\mathcal{B}_{00}^{(4)}\left(\beta^2X^2+\frac{Y^2}{2}\right)+\mathcal{B}_{20}^{(4)}\cos(2mX)+\mathcal{B}_{02}^{(4)}\cos(2mY)\right.\\&\left.+\mathcal{B}_{22}^{(4)}\cos(2mX)\cos(2nY)\right]+O(\epsilon^5)\end{aligned}\tag{A4}$$

in which

$$\alpha=\sqrt{\frac{a}{2}}\quad,\quad a=\sqrt{\frac{1-2\bar{\tau}\mathcal{G}_1}{\mathcal{G}_1\mathcal{G}_4}}$$

The periodicity condition yields

$$\mathcal{A}_{00}^{(0)}=0\tag{A5}$$

$$\mathcal{A}_{00}^{(3/2)}=\frac{2}{3}3^{1/4}\mathcal{P}_q\left(\frac{2\vartheta_1-\vartheta_2}{1-2\bar{\tau}\vartheta_1}\right)-\left(\frac{\vartheta_6\left(\vartheta_1-\vartheta_2\right)\mathcal{V}-2\bar{\tau}\vartheta_7\left(\vartheta_1-\vartheta_2\right)}{1-2\bar{\tau}\vartheta_1}\right)\in^{-1/2} \tag{A6}$$

$$\mathcal{A}_{00}^{(2)}=0 \tag{A7}$$

$$\mathcal{A}_{00}^{(4)}=\frac{2\bar{\tau}\vartheta_2 m^2+\beta^2 n^2\left(1-2\bar{\tau}\vartheta_1\right)}{8\left(1-2\bar{\tau}\vartheta_1\right)}\left(A_{11}^{(2)}\right)^2 \tag{A8}$$

The parameters in Eqs. (37) to (40) are as follow

$$\mathcal{P}_q^{(0)}=K_0K_1\beta^2+K_2\beta^2\in^2 \tag{A9}$$

$$\mathcal{P}_q^{(2)}=8K_1K_3K_8\beta^2+\frac{8K_1K_3\beta^2\left(K_0K_1K_7\beta^2+K_0K_3K_6\right)}{K_0K_1\beta^2-K_6}+\frac{4K_1K_3\beta^2\left(K_0K_7+K_0^2K_3\right)}{K_0K_1\beta^2-K_6}+16K_0K_3K_4\beta^2+\frac{4K_0K_1K_3K_{10}\beta^2}{K_0K_5+K_9} \tag{A10}$$

$$\delta_q^{(0)}=\left[\frac{3^{3/4}}{2}\bar{\tau}\vartheta_6\left(\vartheta_1-\vartheta_2\right)\right]\in^{-1/2}+\left[\frac{2\bar{\tau}^2\vartheta_2\left(\vartheta_1-\vartheta_2\right)}{\beta^2\left(1-2\bar{\tau}\vartheta_1\right)}\right]\in^{-1}+\left[\frac{\vartheta_1}{2}-\vartheta_2-\bar{\tau}\vartheta_2\left(\frac{2\vartheta_1-\vartheta_2}{1-2\bar{\tau}\vartheta_1}\right)+\left(\frac{2\vartheta_1\vartheta_2-\vartheta_2^2}{\pi\alpha\vartheta_1\left(1-2\bar{\tau}\vartheta_1\right)}\right)\in^{1/2}\right]\mathcal{P}_q+\left[\left(\frac{3^{1/4}\alpha\left(2\vartheta_1-\vartheta_2\right)^2}{6\pi\left(1-2\bar{\tau}\vartheta_1\right)}\right)\in\right]\mathcal{P}_q^2 \tag{A11}$$

$$\delta_q^{(2)}=\left[\frac{3^{3/4}}{32}\left(\left(m^2\left(1-2\bar{\tau}\vartheta_1\right)+2\bar{\tau}\vartheta_2\beta^2n^2\right)-\frac{4\bar{\tau}^2\vartheta_2^2m^2+2\bar{\tau}\vartheta_2\beta^2n^2\left(1-2\bar{\tau}\vartheta_1\right)}{1-2\bar{\tau}\vartheta_1}\right)\right]\in^{-3/2} \tag{A12}$$

$$\delta_q^E=\frac{3^{3/4}}{2}\left(\frac{\vartheta_6\left(\vartheta_1-\vartheta_2\right)\mathcal{V}}{2}\right)\in^{-1/2} \tag{A13}$$

where K_i (i=0,…,10) are the parameters in terms of ϑ_1, ϑ_2, ϑ_3, ϑ_4, ϑ_5, m, n, β, and l obtained via the sets of perturbation equations.

$$\mathcal{S}_1=-\left[\left(\frac{2\vartheta_1-\vartheta_2}{1-2\bar{\tau}\vartheta_1}\right)\left(\mathcal{P}_q^{(2)}\right)\right] \tag{A14}$$

$$\mathcal{S}_2=-\left(\frac{2\vartheta_1-\vartheta_2}{1-2\bar{\tau}\vartheta_1}\right)\left(\mathcal{P}_q^{(0)}\right)-\left(\frac{2\bar{\tau}\vartheta_7\left(\vartheta_1-\vartheta_2\right)--\vartheta_6\left(\vartheta_1-\vartheta_2\right)\mathcal{V}}{1-2\bar{\tau}\vartheta_1}\right)\in \tag{A15}$$

References

[1] Y.G. Hu, K.M. Liew, Q. Wang, X.Q. He, B.I. Yakobson. Nonlocal shell model for elastic wave propagation in single- and double-walled carbon nanotubes. *Journal of the Mechanics and Physics of Solids*, 56 (2008) 3475-3485.

[2] H.-S. Shen, C.L. Zhang.Torsional buckling and postbuckling of double-walled carbon nanotubes by nonlocal shear deformable shell model. *Composite Structures*, 92 (2010) 1073-1084.

[3] B. Wang, J. Zhao, Sh. Zhou. A micro scale Timoshenko beam model based on strain gradient elasticity theory. *European Journal of Mechanics – A/Solids*, 29 (2010) 591-599.

[4] R. Ansari, S. Sahmani, B. Arash. Nonlocal plate model for free vibrations of single-layered graphene sheets. *Physics Letters A*, 375 (2010) 53-62.

[5] F. Khademolhosseini, R.K.N.D. Rajapakse, A. Nojeh. Torsional buckling of carbon nanotubes based on nonlocal elasticity shell models. *Computational Materials Science*, 48 (2010) 736-742.

[6] H.-S. Shen, C.L. Zhang. Nonlocal beam model for nonlinear analysis of carbon nanotubes on elastomeric substrates. *Computational Materials Science*, 50 (2011) 1022-1029.

[7] S. Ahangar, G. Rezazadeh, R. Shabani, A. Toloei. On the stability of a microbeam conveying fluid considering modified couple stress theory. *International Journal of Mechanics and Materials in Design*, 7 (2011) 327-342.

[8] E. Ghavanloo, S. Ahmad Fazelzadeh. Nonlocal elasticity theory for radial vibration of nanoscale spherical shells. *European Journal of Mechanics – A/Solids*, 41 (2013) 37-42.

[9] H.-S. Shen. Nonlocal shear deformable shell model for torsional buckling and postbuckling of microtubules in thermal environment. *Mechanics Research Communications*, 54 (2013) 83-95.

[10] A. Ghanbarpour Arani, R. Kolahchi, A. Mortazavi. Nonlocal piezoelasticity based wave propagation of bonded double-piezoelectric nanobeam-systems. *International Journal of Mechanics and Materials in Design*, 10 (2014) 179-191.

[11] S. Sahmani, M. Bahrami, R. Ansari. Nonlinear free vibration analysis of functionally graded third-order shear deformable microbeams based on the modified strain gradient elasticity theory. *Composite Structures* 110 (2014) 219-230.

[12] K.B. Mustapha, D. Ruan. Size-dependent axial dynamics of magnetically-sensitive strain gradient microbars with end attachments. *International Journal of Mechanical Sciences*, 94-95 (2015) 96-110.

[13] S. Sahmani, M. Bahrami. Size-dependent dynamic stability analysis of microbeams actuated by piezoelectric voltage based on strain gradient elasticity theory. *Journal of Mechanical Science and Technology*, 29 (2015) 325-333.

[14] M.S. Sari, W.G. Al-Kouz. Vibration analysis of non-uniform orthotropic Kirchhoff plates resting on elastic foundation based on nonlocal elasticity theory.

International Journal of Mechanical Sciences, 114 (2016) 1-11.

[15] M. Aydogdu, M. Arda. Torsional vibration analysis of double walled carbon nanotubes using nonlocal elasticity. *International Journal of Mechanics and Materials in Design*, 12 (2016) 71-84.

[16] S. Sahmani, M.M. Aghdam. Size dependency in axial postbuckling behavior of hybrid FGM exponential shear deformable nanoshells based on the nonlocal elasticity theory. *Composite Structures*, 166 (2017) 104-113.

[17] S. Sahmani, M.M. Aghdam. Nonlinear instability of hydrostatic pressurized hybrid FGM exponential shear deformable nanoshells based on nonlocal continuum elasticity. *Composites Part B: Engineering*, 114 (2017) 404-417.

[18] S. Sahmani, M.M. Aghdam. Temperature-dependent nonlocal instability of hybrid FGM exponential shear deformable nanoshells including imperfection sensitivity. *International Journal of Mechanical Sciences*, 122 (2017) 129-142.

[19] M. Mohammadimehr, H. Mohammadi Hooyeh, H. Afshari, M.R. Salarkia. Free vibration analysis of double-bonded isotropic piezoelectric Timoshenko microbeam based on strain gradient and surface stress elasticity theories under initial stress using differential quadrature method. *Mechanics of Advanced Materials and Structures*, 24 (2017) 1142022.

[20] S. Sahmani, M.M. Aghdam. Nonlinear vibrations of pre- and post-buckled lipid supramolecular micro/nano-tubules via nonlocal strain gradient elasticity theory. *Journal of Biomechanics*, 65 (2017) 49-60.

[21] S. Sahmani, M.M. Aghdam. Nonlocal strain gradient beam model for postbuckling and associated vibrational response of lipid supramolecular protein micro/nano-tubules. *Mathematical Biosciences*, 295 (2018) 24-35.

[22] L. Lu, X. Guo, J. Zhao. Size-dependent vibration analysis of nanobeams based on the nonlocal strain gradient theory. *International Journal of Engineering Science*, 116 (2017) 12-24.

[23] S. Sahmani, M.M. Aghdam. Size-dependent nonlinear bending of micro/nano-beams made of nanoporous biomaterials including a refined truncated cube cell. *Physics Letters A*, 381 (2017) 3818-3830.

[24] S. El-Borgi, P. Rajendran, M.I. Friswell, M. Trabelssi, J.N. Reddy. Torsional vibration of size-dependent viscoelastic rods using nonlocal strain and velocity gradient theory. *Composite Structures*, 186 (2018) 274-292.

[25] S. Sahmani, M.M. Aghdam. Nonlocal strain gradient shell model for axial buckling and postbuckling analysis of magneto-electro-elastic composite nanoshells. *Composites Part B: Engineering*, 132 (2018) 258-274.

[26] S. Sahmani, M.M. Aghdam, T. Rabczuk. Nonlinear bending of functionally graded porous micro/nano-beams reinforced with graphene platelets based upon nonlocal strain gradient theory. *Composite Structures*, 186 (2018) 68-78.

[27] M.E. Gurtin, A.I. Murdoch. A continuum theory of elastic material surface. *Archive for Rational Mechanics and Analysis*, 57 (1975) 291-323.

[28] M.E. Gurtin, A.I. Murdoch. Surface stress in solids. *International Journal of Solids and Structures*, 14 (1978) 431-440.

[29] C.W. Lim, L.H. He. Size-dependent nonlinear response of thin elastic films with nano-scale thickness. *International Journal of Mechanical Sciences*, 46 (2004) 1715-1726.

[30] Z.R. Li, C.W. Lim, L.H. He. Stress concentration around a nano-scale spherical cavity in elastic media: effect of surface stress. *European Journal of Mechanics – A/Solids*, 25 (2006) 260-270.

[31] G.F. Wang, X.Q. Feng. Effects of surface stresses on contact problems at nanoscale. *Journal of Applied Physics*, 101 (2007) 013510.

[32] J. He, C.M. Lilley. Surface effect on the elastic behavior of static bending nanowires. *Nano Letters*, 8 (2008) 1798-1802.

[33] S.G. Mogilevskaya, S.L. Crouch, H.K. Stolarski. Multiple interacting circular nano-inhomogeneities with surface/interface effects. *Journal of the Mechanics and Physics of Solids*, 56 (2008) 2298-2327.

[34] X.J. Zhao, R.K.N.D. Rajapakse. Analytical solutions for a surface-loaded isotropic elastic layer with surface energy effects. *International Journal of Engineering Science*, 47 (2009) 1433-1444.

[35] Y. Fu, J. Zhang, Y. Jiang. Influences of surface energies on the nonlinear static and dynamic behaviors of nanobeams. *Physica E*, 42 (2010) 2268-2273.

[36] R. Ansari, S. Sahmani. Bending behavior and buckling of nanobeams including surface stress effects corresponding to different beam theories. *International Journal of Engineering Science*, 49 (2011) 1244-1255.

[37] R. Ansari, S. Sahmani. Surface stress effects on the free vibration behavior of nanoplates. *International Journal of Engineering Science*, 49 (2011) 1204-1215.

[38] L. Wang. Surface effect on buckling configuration of nanobeams containing internal flowing fluid: A nonlinear analysis. *Physica E*, 44 (2012) 808-812.

[39] H. Liu, H. Liu, J. Yang. Surface effects on the propagation of shear horizontal waves in thin films with nano-scalethickness. *Physica E*, 49 (2013) 13-17.

[40] M.E. Khater, M.A. Eltaher, E. Abdel-Rahman, M. Yavuz. Surface and thermal load effects on the buckling of curved nanowires. *Engineering Science and Technology, an International Journal*, 17 (2014) 279-283.

[41] F. Gao, Q. Cheng, J. Luo. Mechanics of nanowire buckling on elastomeric substrates with consideration of surface stress effects. *Physica E*, 64 (2014) 72-77.

[42] S. Sahmani, M. Bahrami, M.M. Aghdam, R. Ansari. Surface effects on the nonlinear forced vibration response of third-order shear deformable nanobeams. *Composite Structures*, 118 (2014) 149-158.

[43] S. Sahmani, M. Bahrami, R. Ansari. Surface effects on the free vibration behavior of postbuckled circular higher-order shear deformable nanoplates including geometrical nonlinearity. *Acta Astronautica*, 105 (2014) 417-427.

[44] Y.Q. Zhang, M. Pang, W.Q. Chen. Transverse vibrations

of embedded nanowires under axial compression with high-order surface stress effects. *Physica E*, 66 (2015) 238-244.

[45] S. Sahmani, M.M. Aghdam, M. Bahrami. On the free vibration characteristics of postbuckled third-order shear deformable FGM nanobeams including surface effects. *Composite Structures*, 121 (2015) 377-385.

[46] X. Liang, Sh. Hu, Sh. Shen. Surface effects on the post-buckling of piezoelectric nanowires. *Physica E*, 69 (2015) 61-64.

[47] A.A. Abdel Rahman, A.G. El-Shafei, F.F. Mahmoud. Influence of surface energy on the nanoindentation response of elastically-layered viscoelastic materials. *International Journal of Mechanics and Materials in Design*, 12 (2016) 193-209.

[48] S. Sahmani, M.M. Aghdam, A.H. Akbarzadeh. Size-dependent buckling and postbuckling behavior of piezoelectric cylindrical nanoshells subjected to compression and electrical load. *Materials & Design*, 105 (2016) 341-351.

[49] S. Sahmani, M.M. Aghdam. Imperfection sensitivity of the size-dependent postbuckling response of pressurized FGM nanoshells in thermal environments. *Archives of Civil and Mechanical Engineering*, 17 (2017) 623-638.

[50] S. Sahmani, M.M. Aghdam, M. Bahrami. Surface free energy effects on the postbuckling behavior of cylindrical shear deformable nanoshells under combined axial and radial compressions. *Meccanica*, 52 (2017) 1329-1352.

[51] S. Sahmani, M.M. Aghdam, M. Bahrami. Nonlinear buckling and postbuckling behavior of cylindrical shear deformable nanoshells subjected to radial compression including surface free energy effects. *Acta Mechanica Solida Sinica*, 30 (2017) 209-222.

[52] S. Sahmani, M.M. Aghdam, M. Bahrami. An efficient size-dependent shear deformable shell model and molecular dynamics simulation for axial instability analysis of silicon nanoshells. *Journal of Molecular Graphics and Modelling*, 77 (2017) 263-279.

[53] L.H. Donnell. Beam, *plates and shells*. McGraw-Hill, New York, USA, (1976) 377-445.

[54] H.-S. Shen, T.-Y. Chen. A boundary layer theory for the buckling of thin cylindrical shells under external pressure. *Applied Mathematics and Mechanics*, 9 (1988) 557-571.

[55] H.-S. Shen. Boundary layer theory for the buckling and postbuckling of an anisotropic laminated cylindrical shell, Part II: Prediction under external pressure. *Composite Structures*, 82 (2008) 362-370.

[56] H.-S. Shen. Postbuckling of 3D braided composite cylindrical shells under combined external pressure and axial compression in thermal environments. *International Journal of Mechanical Sciences*, 50 (2008) 719-731.

[57] H.-S. Shen, Y. Xiang. Postbuckling behavior of functionally graded graphene-reinforced composite laminated cylindrical shells under axial compression in thermal environments. *Computer Methods in Applied Mechanics and Engineering*, 330 (2018) 64-82.

[58] H.-S. Shen, Y. Xiang. Postbuckling of functionally graded graphene-reinforced composite laminated cylindrical shells subjected to external pressure in thermal environments. *Thin-Walled Structures*, 124 (2018) 151-160.

[59] S. Sahmani, M.M. Aghdam. Size-dependent axial instability of microtubules surrounded by cytoplasm of a living cell based on nonlocal strain gradient elasticity theory. *Journal of Theoretical Biology*, 422 (2017) 59-71.

[60] S. Sahmani, M.M. Aghdam. Nonlinear instability of axially loaded functionally graded multilayer graphene platelet-reinforced nanoshells based on nonlocal strain gradient elasticity theory. *International Journal of Mechanical Sciences*, 131-132 (2017) 95-106.

[61] S. Sahmani, M.M. Aghdam. A nonlocal strain gradient hyperbolic shear deformable shell model for radial postbuckling analysis of functionally graded multilayer GPLRC nanoshells. *Composite Structures*, 178 (2017) 97-109.

[62] S. Sahmani, M.M. Aghdam. Nonlocal strain gradient beam model for nonlinear vibration of prebuckled and postbuckled multilayer functionally graded GPLRC nanobeams. *Composite Structures*, 179 (2017) 77-88.

[63] G.Y. Huang, S.W. Yu. Effect of surface piezoelectricity on the electromechanical behavior of piezoelectric ring. *Physics of Status Solidi B*, 243 (2006) R22-R24.

[64] Z. Yan, L.Y. Jiang. Surface effects on the electromechanical coupling and bending behaviours of piezoelectric nanowires. *Journal of Physics D*, 44 (2011) 075404.

[65] Z. Yan, L.Y. Jiang. The vibrational and buckling behaviors of piezoelectric nanobeams with surface effects. *Nanotechnology*, 22 (2011) 245703.

[66] P. Mirfakhraei, D. Redekop. Buckling of circular cylindrical shells by the differential quadrature method. *International Journal of Pressure Vessels and Piping*, 75 (1998) 347-353.

Please cite this article using:

S. Sahmani, M.M. Aghdam, A.H. Akbarzadeh, Surface Stress Size Dependency in Nonlinear Instability of Imperfect Piezoelectric Nanoshells under Combination of Hydrostatic Pressure and Lateral Electric Field, *AUT J. Mech. Eng.*, 2(2) (2018) 177-190.

DOI: 10.22060/ajme.2018.13624.5687